MOLECULAR AND CELLULAR BIOLOGY, Jan. 2011, p. 63–80 Vol. 31, No. 1
0270-7306/11/$12.00 doi:10.1128/MCB.00468-10

Requirement for Class II Phosphoinositide 3-Kinase C2α in Maintenance of Glomerular Structure and Function▽

David P. Harris,[1]* Peter Vogel,[1] Marie Wims,[1] Karen Moberg,[1] Juliane Humphries,[1] Kanchan G. Jhaver,[1] Christopher M. DaCosta,[1] Melanie K. Shadoan,[1]‡ Nianhua Xu,[1] Gwenn M. Hansen,[1] Sanjeevi Balakrishnan,[2] Jan Domin,[2]† David R. Powell,[1] and Tamas Oravecz[1]

Lexicon Pharmaceuticals, Inc., 8800 Technology Forest Place, The Woodlands, Texas 77381,[1] and Renal Section, Division of Medicine, Imperial College London, Du Cane Road, London W12 0NN, United Kingdom[2]

Received 19 April 2010/Returned for modification 23 May 2010/Accepted 13 October 2010

An early lesion in many kidney diseases is damage to podocytes, which are critical components of the glomerular filtration barrier. A number of proteins are essential for podocyte filtration function, but the signaling events contributing to development of nephrotic syndrome are not well defined. Here we show that class II phosphoinositide 3-kinase C2α (PI3KC2α) is expressed in podocytes and plays a critical role in maintaining normal renal homeostasis. PI3KC2α-deficient mice developed chronic renal failure and exhibited a range of kidney lesions, including glomerular crescent formation and renal tubule defects in early disease, which progressed to diffuse mesangial sclerosis, with reduced podocytes, widespread effacement of foot processes, and modest proteinuria. These findings were associated with altered expression of nephrin, synaptopodin, WT-1, and desmin, indicating that PI3KC2α deficiency specifically impacts podocyte morphology and function. Deposition of glomerular IgA was observed in knockout mice; importantly, however, the development of severe glomerulonephropathy preceded IgA production, indicating that nephropathy was not directly IgA mediated. PI3KC2α deficiency did not affect immune responses, and bone marrow transplantation studies also indicated that the glomerulonephropathy was not the direct consequence of an immune-mediated disease. Thus, PI3KC2α is critical for maintenance of normal glomerular structure and function by supporting normal podocyte function.

Phosphoinositide 3-kinase (PI3K) enzymes are a family of lipid kinases that phosphorylate the 3′ position of the inositol ring on phosphatidylinositol (PI) and higher-phosphorylated polyphosphoinositides (19, 27, 51). The lipid products generated by PI3Ks serve as important intracellular second messengers that interact with effector proteins, which include Ser/Thr kinases and Tec family kinases, leading to their recruitment to the plasma membrane and subsequent activation. Consequently, PI3K enzymes play an important role in regulating downstream signaling cascades that control diverse cellular functions, including proliferation, migration, apoptosis, and glucose metabolism (19, 27, 51). Mutation or aberrant expression of either the PI3K enzymes or the corresponding PI phosphatases, such as phosphatase and tensin homolog (PTEN) and Src homology 2 domain-containing inositol 5-phosphatase (SHIP), has been implicated in a number of diseases, including cancer, diabetes, and inflammation (27, 40).

The PI3K family of enzymes is divided into 3 classes based on structure and preferred substrate specificity. Class I PI3Ks are heterodimers, composed of one of four different 110-kDa catalytic isoforms coupled with one of five smaller regulatory subunits. Their product is $PI(3,4,5)P_3$, which is rapidly and transiently produced after stimulation (19). The role of class I PI3Ks in cellular activation, particularly in lymphocytes, has been examined in considerable detail, and therapeutic approaches based on targeting class I PI3Ks are currently being evaluated (19, 31). In contrast, less is known about the physiological functions of the three monomeric class II PI3K isoforms, C2α, C2β, and C2γ. In common with the class I enzymes, class II PI3Ks contain Ras-binding, C2-like, and kinase domains (13, 33), while also sharing highly conserved Phox (PX) homology and C2 domains that are unique to the class II isoforms in the PI3K family. The latter domains are located within the C-terminal region of the enzyme, and they mediate protein and phospholipid-binding activities and contain a nuclear localization signal (11, 45). There is one class III PI3K isoform, vesicular protein-sorting protein Vsp34, a monomer involved in intracellular trafficking (19).

Structurally, PI3KC2α differs from all other PI3Ks by containing clathrin-binding, proline-rich, and coiled-coil domains in the N-terminal segment. PI3KC2α is also less sensitive than other PI3K isoforms to the kinase blocking activity of the benchmark PI3K inhibitors wortmannin and LY294002 (13). While the *in vivo* substrates of PI3KC2α have not been identified, *in vitro* it can generate PI(3)P and $PI(3,4)P_2$. PI3KC2α is constitutively associated with phospholipid membranes and has been identified in various intracellular locations, including the *trans*-Golgi network (TGN), endocytic compartments, clathrin-coated vesicles, and nuclear speckles, where it may

* Corresponding author. Mailing address: Lexicon Pharmaceuticals, Inc., 8800 Technology Forest Place, The Woodlands, TX 77381. Phone: (281) 863-3478. Fax: (281) 863-2665. E-mail: dpharris@lexpharma.com.
† Present address: University of Bedfordshire, Luton LU1 3JU, United Kingdom.
‡ Present address: GlaxoSmithKline, Research Triangle Park, NC 27709.
▽ Published ahead of print on 25 October 2010.

associate with factors involved in mRNA metabolism (11, 39, 45). Histological analysis of normal human tissues revealed prominent PI3KC2α expression in fully differentiated, nonproliferating cells, including endothelial cells lining capillaries, testicular Leydig cells, and the glomerular tuft, and in spleen and lymph nodes, where expression was prominent in macrophages and polymorphonuclear leukocytes (16). *Ex vivo* studies indicated that a diverse set of stimuli, including growth factors (4), chemokines (47), cytokines (30), integrins (37), and insulin (8), can induce PI3KC2α activity. PI3KC2α has been shown to regulate the assembly and cellular distribution of clathrin (21). Indeed, it has been suggested that PI3KC2α may control clathrin-dependent trafficking and sorting within the TGN, based on the finding that PI3KC2α expression in COS cells regulates endocytosis of transferrin and localization of mannose-6-phosphate within the TGN (20). PI3KC2α may also play a role in regulating cell survival. For instance, RNA interference (RNAi)-mediated knockdown of *PI3KC2*α expression induced apoptosis via an intrinsic cell death pathway in HeLa (15) and CHO (26) cells, which was associated with increased levels of activated caspase 9 (15). Data from other recent studies have provided evidence that PI3KC2α is a component of diverse cellular processes ranging from neurosecretory granule exocytosis (50) and vascular smooth muscle contraction (53) to insulin signaling (18). The molecular mechanism behind the latter signaling effect is likely related to the PI3KC2α-mediated translocation of the glucose transporter GLUT4 to the plasma membrane (18).

The diverse physiological effects observed at the cellular level make it difficult to deduce the significance of PI3KC2α enzyme expression in mammals and predict the consequences of modulation of PI3KC2α activity *in vivo*. In the present work, we have generated mice deficient in expression of this PI3K isoform. A detailed phenotypic analysis of the knockout (KO) mice revealed that PI3KC2α is essential for normal renal function and, more specifically, for the development and/or maintenance of podocytes, whose damage is an early finding in many human kidney diseases.

MATERIALS AND METHODS

Generation of *PI3KC2*α mutant mice. *PI3KC2*α-null mice were generated by gene trapping as previously described (49). The Lexicon OmniBank embryonic stem cell (ESC) clone OST288105 was selected for microinjection based on sequence similarity to the mouse *PI3KC2*α gene (GenBank accession number NM_011083). The genomic insertion site of the gene trap vector in OST58278 was determined by inverse PCR (Fig. 1A). Mice carrying this mutation were generated by using standard methods of host embryo microinjection of ESCs, chimera production, and germ line transmission. Genotyping and expression analysis of wild-type (WT) and mutant *PI3KC2*α alleles were performed by PCR. Primer sequences used for quantitative PCR (qPCR) analysis are available on request.

All experiments were performed on mice of mixed genetic background (129/SvEvBrd and C57BL/6J) representing both sexes of littermate mutant and WT animals. Procedures involving animals were conducted in conformity with the Institutional Animal Care and Use Committee guidelines in compliance with state and federal laws and the standards outlined in the *Guide for the Care and Use of Laboratory Animals* (34a).

Immunoblotting, immunoprecipitation, and enzyme activity measurements. (i) Western blotting. Cell lysates were prepared from brain and kidney tissues and probed using antibodies (Abs) to PI3KC2α (Ab #1, Fig. 1 [catalog no. 611046; BD Biosciences, San Diego, CA]; Ab #2, Fig. 1 [catalog no. sc-67306; Santa Cruz Biotechnology, Santa Cruz, CA]; and Ab #3, Fig. 1 [47]) and to GAPDH (glyceraldehyde-3-phosphate dehydrogenase) (Bethyl Laboratories, Montgomery, TX), horseradish peroxidase (HRP)-conjugated secondary Abs with appropriate specificity, and an ECL detection system (GE Life Sciences, Pittsburgh, PA).

(ii) Immunoprecipitation and enzyme activity measurements. Liver and kidney tissues were homogenized in ice-cold lysis buffer (10 mM Tris-HCl, pH 7.6, 5 mM EDTA, 50 mM NaCl, 30 mM sodium pyrophosphate, 50 mM NaF, 100 mM Na_3VO_4, 1% Triton X-100, 5 mg/ml antipain, 1 mg/ml pepstatin, 5 mg/ml leupeptin, and 1 mM phenylmethylsulfonyl fluoride [PMSF]). Homogenates were clarified by repeated centrifugation at 13,000 × *g*, and supernatants were then incubated with anti-PI3KC2α Ab (13) for 3 h, followed by incubation with 20 μl protein A-Sepharose for 1 h at 4°C. Phosphoinositide kinase activity in each immunoprecipitate was quantified as previously described (13).

Histology. (i) Immunohistochemistry (IHC). Formalin-perfused and -fixed tissue sections were prepared as described previously (49) and stained with hematoxylin and eosin (H&E), periodic acid-Schiff stain (PAS), or Ab specific for PI3KC2α (47), IgA (Bethyl Laboratories, Montgomery, TX), MECA 32 (BD Biosciences), nephrin (Santa Cruz Biotechnology, Santa Cruz, CA), WT-1 (Santa Cruz), synaptopodin (Life Span Biosciences, Seattle, WA), desmin (Cell Signaling Technology, Danvers, MA), IgG (Vector Laboratories, Burlingame, CA), or Ki-67 (Bethyl Laboratories, Montgomery, TX).

(ii) Immunofluorescence (IF). Anti-IgA–fluorescein isothiocyanate (FITC) (Southern Biotechnology, Birmingham, AL) and goat anti-mouse kappa–Texas Red (Southern Biotechnology) staining was performed on nonperfused frozen tissue sections.

(iii) Electron microscopy. For ultrastructural analysis, selected sections of kidney perfused with 3.5% glutaraldehyde were incubated in 2% osmium tetroxide, stained with 2% uranyl acetate, dehydrated in graded ethanols, and embedded in Spurr's resin. Semithin sections were stained with 1% toluidine blue. Ultrathin sections were poststained with 4% methanolic uranyl acetate and Venable's lead citrate and examined with a transmission electron microscope.

Clinical chemistry and renal function and hematology assays. Serum chemistry and urine parameters were measured with a Cobas Integra 400 autoanalyzer (Roche, Indianapolis, IN), and complete blood cell count and fluorescence-activated cell sorter (FACS) analysis were performed as described earlier (49). For urinalysis, 24-h urine samples were collected for four consecutive days from mice individually housed in metabolic cages and acclimatized for 1 week prior to the start of urine collection. The creatinine clearance rate was estimated based on serum creatinine concentration (Creatinine plus version 2; Roche) and average daily urine creatinine excretion. The coefficient of variation for creatinine excretion across 4 days was measured to confirm complete urine collection and was ≤25%. Proteinuria was analyzed by running urine samples from WT and KO mice on 10% SDS-polyacrylamide gels. Albumin was included as a control. Proteins were visualized on gels by Coomassie blue staining.

Body composition analysis. Noninvasive measurements of body composition were made using quantitative magnetic resonance technology as described previously (7).

Measurements of serum Ig, autoantibodies, and immune complexes. Reagents from Southern Biotechnology and Alpha Diagnostics (San Antonio, TX) were used to measure Ig and autoantibodies by using standard enzyme-linked immunosorbent assay (ELISA) procedures. For measurement of IgA-fibronectin, ELISA plates (5 μg/ml) were coated with rabbit anti-mouse fibronectin (Chemicon, Temecula, CA), and serum was diluted 1/100 and added for 2 h, followed by addition of goat anti-mouse IgA–HRP (Southern Biotechnology). Semiquantitative measurement of circulating immune complex (CIC) was performed using an ELISA kit from Alpha Diagnostics (catalog no. 5900) in accordance with the manufacturer's instructions.

BM transplantation. Recipient mice, at 12 weeks of age, were irradiated and transplanted with bone marrow (BM) from 12-week-old donor mice as described before (2). Reconstitution was monitored by performing quantitative PCR for *Neo* (in the trapping cassette) on peripheral blood leukocytes from retroorbital bleeds taken 12 to 16 weeks after transplantation. The percentage of cells derived from donor BM was always >90% in the animals that had undergone BM reconstitution.

Immune function assays. (i) Cell proliferation. Splenocytes were cultured for 48 h with stimuli. The rate of cell proliferation was monitored in triplicate samples by [^{3}H]thymidine ([^{3}H]TdR) incorporation (0.5 μCi/well) during the last 12 h of the cultures.

(ii) Cytokine response. Concentrations of cytokines in cell culture supernatants and peritoneal lavage fluid were measured using cytometric bead array (CBA) mouse inflammation kits following the manufacturer's instructions (BD Biosciences).

(iii) Ab response to OVA. Animals were injected intraperitoneally (i.p.) with 100 μg of chicken ovalbumin (OVA) (Sigma-Aldrich) emulsified in complete

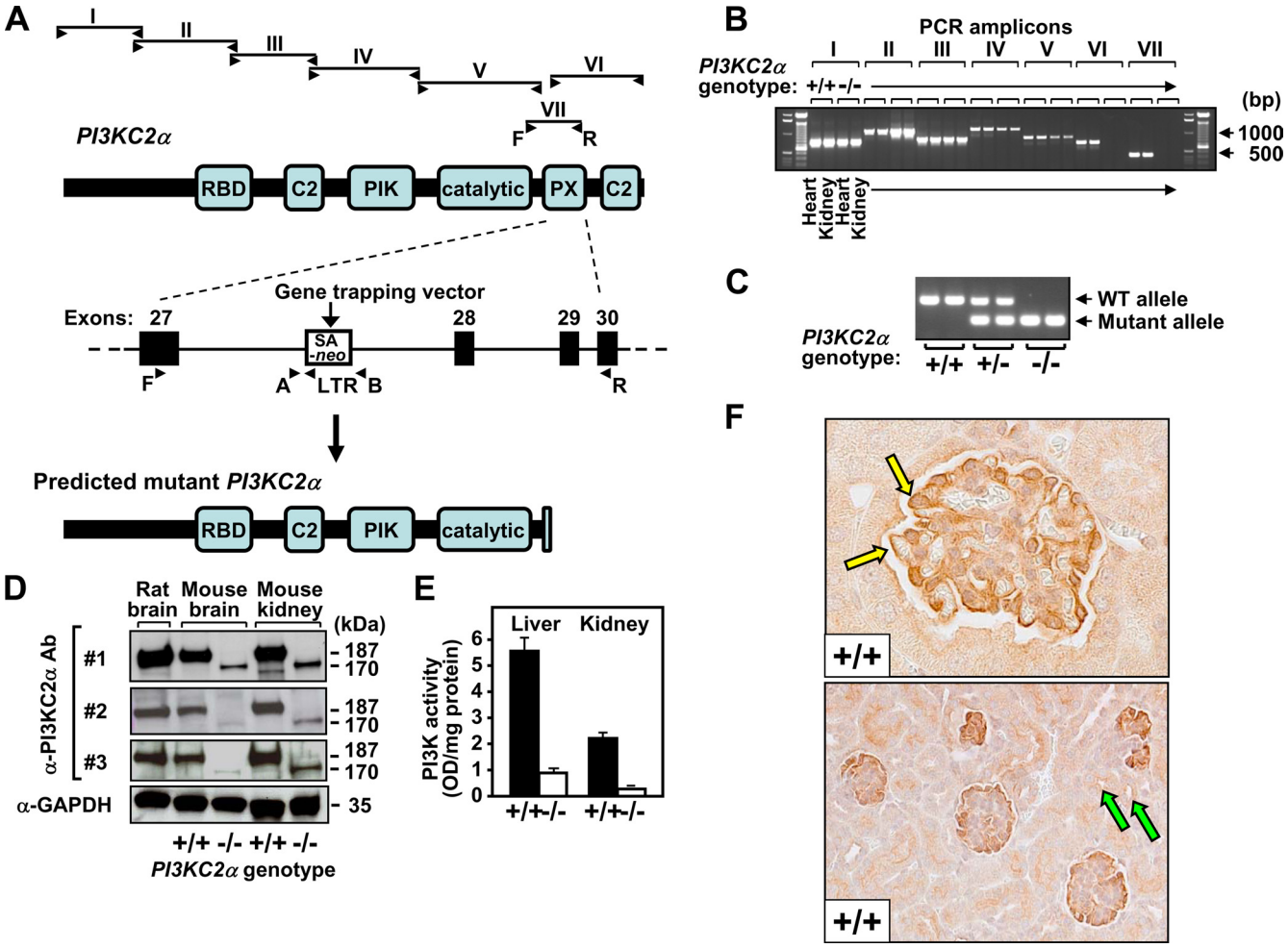

FIG. 1. Generation of *PI3KC2*α mutant mice. (A) Gene trap mutation and location of primers for genotyping strategy and expression analysis of the *PI3KC2*α gene. Arrowheads indicate transcription start sites. Primers A-B and F-R flank the insertion site of the gene trap vector and amplify PCR products from the WT allele. The long terminal repeat (LTR) primer, complementary to the gene trap vector, amplifies the mutant allele in conjunction with primer A. SA, splice acceptor sequence; *neo*, neomycin resistance gene. (B) Gene transcripts were detected in the designated tissues by reverse transcriptase PCR (RT-PCR) using primers that amplify the indicated regions. (C) Genotypic analysis of mice at the *PI3KC2*α locus was performed by screening genomic DNA isolated from tail biopsy samples. (D) Immunoblotting of tissue lysates with Abs as indicated. Anti-PI3KC2α (α-PI3KC2α) Ab #1 and Ab #2 were obtained from BD Biosciences and Santa Cruz Biotechnology, respectively, and anti-PI3KC2α Ab #3 has been described previously (47). (E) Specific enzyme activities of PI3KC2α immunoprecipitates from the indicated tissues (n = 5). OD, optical density. (F) PI3KC2α IHC of representative WT kidney sections with anti-PI3KC2α Ab #3, showing positive staining of podocytes (yellow arrows, ×100) and the tubular epithelium (green arrows, ×40).

Freund's adjuvant (Sigma-Aldrich). Serum titers of anti-OVA Abs (IgG1 and IgG2a subclasses) were measured by ELISA 14 days after immunization. Custom-formulated plates surface coated with 0.01 mg/ml OVA were purchased from BD Biosciences (catalog no. 353279). Sera were diluted in sample buffer (Tris-buffered saline [TBS] with 1% nonfat dry milk) and incubated on the plates for 1 h at room temperature in a 100-μl volume. For detection of anti-OVA Ab, HRP-conjugated goat anti-mouse IgG1 and IgG2a Abs were used at a 1:5,000 dilution (Southern Biotechnology). Plates were washed four times with TBS supplemented with Tween 20 after each Ab incubation. Enzyme reactions were followed by addition of 3,3′,5,5′-tetramethylbenzidine as a substrate.

(iv) TGF-β measurement. Levels of transforming growth factor β1 (TGF-β1) in serum were measured using an ELISA kit from Promega (Madison, WI) according to the manufacturer's instructions.

(v) LPS-induced immunoglobulin production. Splenocytes (10^6/ml) were stimulated *in vitro* with 2.5 μg/ml lipopolysaccharide (LPS) (Sigma-Aldrich) for 10 days; supernatants were then harvested, and immunoglobulin production was measured by ELISA. ELISA plates were coated with isotype-specific primary Ab (5 μg/ml), supernatants were diluted 1/5 or 1/10 in blocking buffer, and HRP-labeled goat anti-mouse secondary Abs were used at a 1:1,000 dilution. All Abs were from Southern Biotechnology. Plates were washed four times with TBS supplemented with Tween 20 after each Ab incubation. Enzyme reactions were followed by addition of 3,3′,5,5′-tetramethylbenzidine as a substrate.

(vi) Zymosan-induced peritoneal inflammation. Mice were injected i.p. with 1 ml of 1 mg/ml zymosan (Invitrogen, Carlsbad, CA). After 4 h, animals were euthanized and the peritoneal cavity was flushed with 5 ml phosphate-buffered saline (PBS) to collect lavage fluid, which was analyzed using a Cell-Dyn 3500R automated hematology analyzer (Abbott Diagnostics, Abbott Park, IL).

(vii) In vivo apoptosis assay. Mice were injected i.p. with Ab to CD3 (0.5 μg/g body weight) (BD Biosciences). After 48 h, animals were euthanized, spleens were removed, and single cell suspensions of splenocytes were examined by FACS analysis as described previously (49). For annexin V and 7-aminoactinomycin D staining, cell suspensions were incubated at room temperature with the reagents (BD Biosciences) for 15 min after the Ab staining step.

(viii) Contact hypersensitivity assay. Mice were sensitized with 3% oxazolone (Sigma-Aldrich, St. Louis, MO), applied to the lower back and right rear footpad. After 6 days, mice were challenged with 1% oxazolone applied to both ears. Ear swelling was measured at various time points by using a Käfer SPI thickness micrometer gauge. Data for the two ears were averaged, and ear swelling was

calculated by subtracting the baseline values registered before sensitization from the values of subsequent measurements.

Statistical analyses. Analysis of the survival data employed the chi-square test. For other data, statistical significance of group differences was evaluated by the unpaired, two-tailed, Student *t* test. A *P* value of <0.05 was considered significant.

RESULTS

PI3KC2α is essential for normal growth and survival. *PI3KC2*α-null mice were derived from the Lexicon OmniBank embryonic stem cell (ESC) clone OST288105 (49). Inverse PCR of genomic DNA isolated from PI3KC2α ESCs identified a gene trap vector insertion within intron 27 of the mouse *PI3KC2*α gene (Fig. 1A). Mice heterozygous for the *PI3KC2*α deletion (*PI3KC2*$\alpha^{+/-}$) were fertile and were intercrossed to obtain homozygous progeny. The average litter size of *PI3KC2*$\alpha^{+/-}$ animals (8 pups) was not different from that of other KO lines maintained in our facility. However, increased cannibalism of progeny was observed prior to genotyping (day 14), and ratios of the three possible genotypes deviated slightly, but significantly, from the normal Mendelian (1:2:1) distribution (26.8% WT, 52.0% *PI3KC2*$\alpha^{+/-}$, and 21.2% *PI3KC2*$\alpha^{-/-}$; $n = 1{,}113$; $P = 0.01$). Successful targeting of the *PI3KC2*α gene in KO mice was confirmed by expression analysis of the gene transcript (Fig. 1B and C), Western blot analysis of the PI3KC2α protein (Fig. 1D), and enzyme activity measurements (Fig. 1E). As expected from the C-terminal location of the targeting vector insertion, only wild-type (WT) cells expressed full-length *PI3KC2*α transcripts, whereas KO tissues contained truncated gene products, as determined by using overlapping gene-specific primers (Fig. 1B and C). The latter data raised the possibility that truncated PI3KC2α proteins might be expressed in *PI3KC2*$\alpha^{-/-}$ mice. Therefore, we performed Western blot analysis of WT and KO tissue lysates by using 3 different Abs to N-terminal epitopes of PI3KC2α encoded by sequences upstream of the vector insertion site. The staining patterns were similar with all 3 Abs, which detected a full-length PI3KC2α protein with the expected apparent molecular mass of ~187 kDa in brain and kidney tissues of WT, but not KO, animals (Fig. 1D). In contrast, the KO tissues expressed an ~170-kDa protein corresponding to a PI3KC2α form that lacked a 267-amino-acid segment encompassing the C-terminal PX and C2 domains, as expected from the targeting vector insertion into the *PI3KC2*α gene. However, the relative intensity of this truncated KO protein signal was considerably lower than that of the WT full-length proteins (Fig. 1D). In addition, cell lysates of KO tissues contained significantly less PI3K enzyme activity than did WT tissues (Fig. 1E). Finally, a polyclonal Ab to PI3KC2α demonstrated the presence of PI3K in podocytes by immunohistochemistry (Fig. 1F). Previously reported immunohistochemical analysis of kidney tissue indicated that PI3KC2α is expressed in the glomerular tuft, predominantly in the visceral podocyte layer (16). Our IHC studies confirmed that PI3KC2α is strongly expressed in podocytes and also showed expression multifocally in the proximal convoluted tubule epithelium in the kidney (Fig. 1F).

Analysis of survival of young *PI3KC2*$\alpha^{-/-}$ animals indicated that PI3KC2α was essential for normal postnatal development (Fig. 2A), and as mice aged, the KO animals became progressively sick and noticeably smaller than their WT littermates

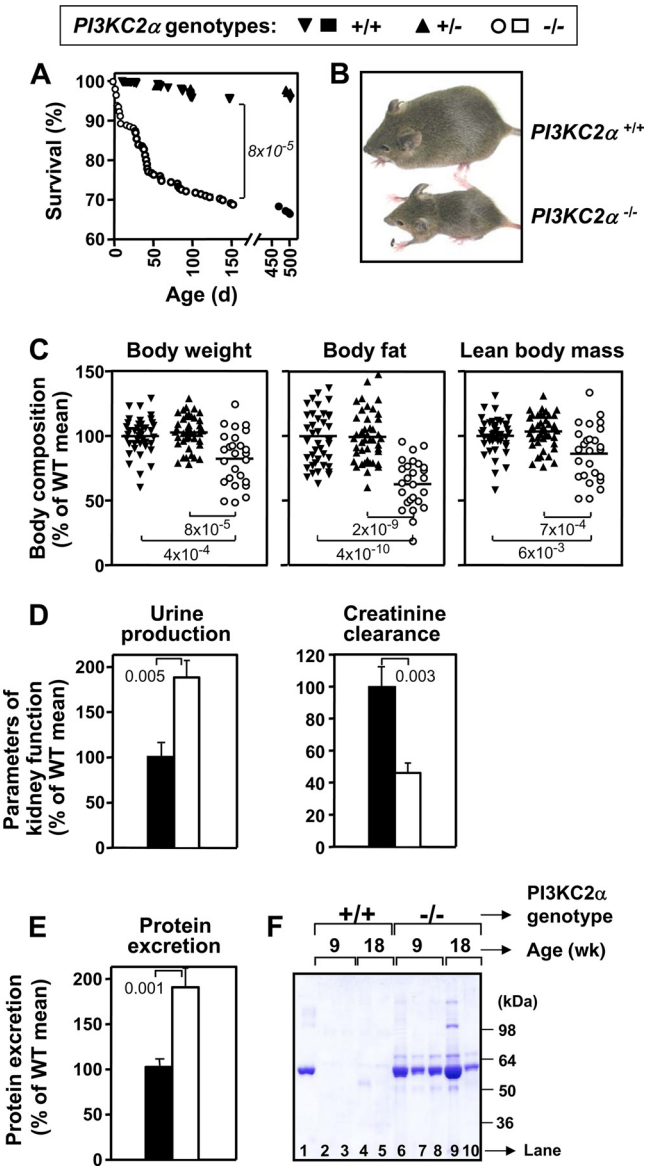

FIG. 2. *PI3KC2*α deficiency elicits clinical signs of kidney failure. (A) Survival curves for mice of the indicated genotypes ($n = >200$ mice per cohort). d, days. (B) Stunted growth of *PI3KC2*$\alpha^{-/-}$ mice at 4 weeks of age. (C) Quantitative magnetic resonance analysis was performed on mice at 6 weeks of age. Data were normalized to the mean of the WT values, and horizontal lines depict the mean of the normalized data for each indicated genotype. The following measured values correspond to 100%: body weight, 21.45 g; body fat, 3.45 g; lean body mass, 18.05 g. (D and E) Parameters of kidney function of mice with the indicated genotypes at 6 weeks of age ($n = 7$ to 14 mice per cohort). Data were normalized to the mean of the WT values and are presented as means ± standard errors of the means (SEM). The following measured values correspond to 100%: urine volume, 2.3 ml/day; creatinine clearance, 311.7 μl/min; protein excretion, 8.3 mg/day. Numbers above the bars indicate *P* values comparing the indicated groups. (F) Proteins in urine samples from mice of the indicated genotypes were visualized by Coomassie blue staining after electrophoretic separation. Lane 1 is an albumin control (3 μg).

(Fig. 2B). At 4 to 6 weeks of age, the body weight of *PI3KC2*$\alpha^{-/-}$ mice was significantly lower than that of WT mice, due to reduced body fat and lean body mass (Fig. 2C). Approximately 30% of *PI3KC2*$\alpha^{-/-}$ mice died by 6 months of

TABLE 1. Deletion of PI3KC2α alters serum chemistry and hematology values consistent with renal disease

Measured parameter	Result[a] for:	
	PI3KC2$\alpha^{+/+}$ mice (n = 8)	*PI3KC2*$\alpha^{-/-}$ mice (n = 14)
Blood chemistry		
Alanine transferase (U/liter)	40.8 ± 7.3	29.7 ± 6.7
Alkaline phosphatase (U/liter)	138.6 ± 15.2	256.1 ± 28.4**
Bilirubin (mg/dl)	0.3 ± 0.0	0.2 ± 0.0*
BUN (mg/dl)	28.0 ± 1.7	74.5 ± 14.2*
Calcium (mg/dl)	9.9 ± 0.2	11.0 ± 0.2**
Chloride (mM)	110.2 ± 0.5	110.9 ± 0.8
Cholesterol (mg/dl)	166.0 ± 32.1	254.1 ± 22.4*
Creatinine (mg/dl)	0.1 ± 0.0	0.2 ± 0.0**
Globulin (mg/dl)	1.9 ± 0.1	2.3 ± 0.1*
Glucose (mg/dl)	147.0 ± 6.6	136.3 ± 6.9
Potassium (mM)	4.2 ± 0.1	4.6 ± 0.1**
Sodium (mM)	146.5 ± 0.4	146.5 ± 0.4
Phosphate (mg/dl)	6.7 ± 0.3	8.0 ± 0.2**
Total protein (g/dl)	5.3 ± 0.1	5.1 ± 0.1
Triglycerides (mg/dl)	56.5 ± 8.4	75.1 ± 11.9
Uric acid (mg/dl)	1.2 ± 0.2	0.9 ± 0.0
Hematology		
Hb (g/dl)	15.3 ± 0.2	12.6 ± 1.1**
Hematocrit (%)	55.1 ± 1.0	46.5 ± 3.9**
Mean platelet vol (fl)	4.2 ± 0.0	4.5 ± 0.1**
Platelets ($\times 10^{-6}$/ml)	539.1 ± 15.1	748.0 ± 124.0*
RBCs ($\times 10^{-9}$/ml)	10.1 ± 0.1	8.4 ± 0.7*

[a] Values for mice at 6 weeks of age. *, $P \leq 4 \times 10^{-2}$; **, $P \leq 4 \times 10^{-3}$.

age, while the death rate was 5% among the WT littermates (Fig. 2A). Growth rate and body composition of heterozygous *PI3KC2*$\alpha^{+/-}$ mice were normal; therefore, they were not routinely included in additional studies.

Blood and urine parameters demonstrate renal failure in *PI3KC2*$\alpha^{-/-}$ mice. The failure to thrive, lean phenotype, and increased mortality observed in *PI3KC2*$\alpha^{-/-}$ mice suggested that these mice might suffer from a chronic illness, so hematologic and metabolic evaluation of mice at different stages of disease development was initiated. A wide array of serum chemistry and hematology parameters showed significant deviation from normal values in *PI3KC2*$\alpha^{-/-}$ mice, including increased serum creatinine, blood urea nitrogen (BUN), and potassium, phosphate, and alkaline phosphatase concentrations, decreased hemoglobin (Hb) levels, lower red blood cell (RBC) counts, and elevated platelet numbers (Table 1 and data available on request). Because such a blood profile is highly suggestive of kidney failure, mice were housed individually in metabolic cages for 24 h to perform tests for renal function (Fig. 2D and E). The test results confirmed the presence of renal failure in *PI3KC2*$\alpha^{-/-}$ mice, as they showed markedly decreased creatinine clearance and polyuria. Furthermore, KO mice exhibited mild, yet highly consistent, proteinuria, which was present in younger, 4- to 6-week-old mice and in older mice (Fig. 2E and F).

PI3KC2α deficiency leads to glomerulonephropathy. Gross and histological lesions were not immediately apparent in kidneys of 3-week-old KO mice (Fig. 3A and B). However, compared directly with those of age-matched WT littermates, the glomeruli of KO mice were enlarged and contained increased mesangium, which was more easily appreciated following specific immunohistochemical staining of podocytes with synaptopodin (Fig. 3C to F). In WT glomeruli, synaptopodin immunolabeling of podocyte foot processes was characterized by thin linear staining along glomerular basement membranes (GBM) of capillary loops throughout the glomerulus, with linear bands and capillaries being separated by narrow cords of mesangial cells (Fig. 3E). In contrast, most synaptopodin-stained glomeruli in 3-week-old KO mice had a cerebriform appearance due to the increased mesangium and restriction of the linear synaptopodin staining to podocyte foot processes lining the visceral surface of Bowman's space; synaptopodin generally did not extend deeply into the glomerular tuft (Fig. 3F).

In comparison to the near-normal appearance of kidneys at 3 weeks of age, severe renal lesions were present in recently weaned, 4-week-old KO mice (Fig. 4A and B), with crescent formation, glomerular adhesions associated with widespread tubular dilation, and eosinophilic casts indicative of glomerular leakage and proteinuria. The levels of severity of glomerular lesions in KO mice were highly variable, but glomerular crescents were most abundant in the midcortical and juxtaglomerular regions (Fig. 4C). Synaptopodin expression was reduced or absent in areas of crescent formation and sclerosis (Fig. 4D), and in most glomeruli, the marked interruptions and coarse granulations produced a patchy staining pattern (Fig. 4E). In contrast, synaptopodin labeling in the immature small subcortical glomeruli was linear and extensive, suggesting that podocyte coverage of these glomeruli was nearer to normal (Fig. 4F).

By 13 weeks, the kidneys of *PI3KC2*$\alpha^{-/-}$ mice were distinctly pale and often smaller than kidneys from *PI3KC2*$\alpha^{+/+}$ mice (data available on request). Histochemical staining of kidney sections from 13-week-old KO mice revealed a range of lesions in affected glomeruli, from minimal-change nephropathy (MCN) and focal segmental glomerulosclerosis (FSGS) in subcortical glomeruli to diffuse mesangial sclerosis (DMS) of most cortical and juxtaglomerular glomeruli. Mesangial cell hypertrophy was the earliest structural change detected in glomeruli. Although DMS and associated tubulointerstitial disease were the predominant lesions in adult mice, less affected subcortical glomeruli showed only mild expansion of the mesangial matrix. At all ages examined, the expansion of the mesangial matrix was accompanied by narrowing of capillary lumens. In many glomeruli, podocytes were reduced in number, while in others the remaining podocytes were hypertrophic. In the 13-week-old mice, many of the more severely affected glomeruli had segmentally or globally collapsed capillary loops, while diffusely sclerotic glomeruli often developed circumferential fibrocellular crescents (Fig. 5A to F). In kidneys at 13 weeks of age, synaptopodin expression was reduced or absent in sclerotic juxtaglomerular and cortical glomeruli, but in the later-developing subcortical glomeruli, linear staining along capillary basement membranes demonstrated that these were less severely affected (Fig. 5G and H). Ultrastructural analysis of kidneys revealed decreased numbers of podocytes and widespread but incomplete effacement of foot processes, with swelling or disappearance of primary processes, in KO mice. Endothelial cells and glomerular basement membranes (GBM) were generally normal, although the GBM were sometimes folded (Fig. 6). Thus, histological analysis revealed a severe

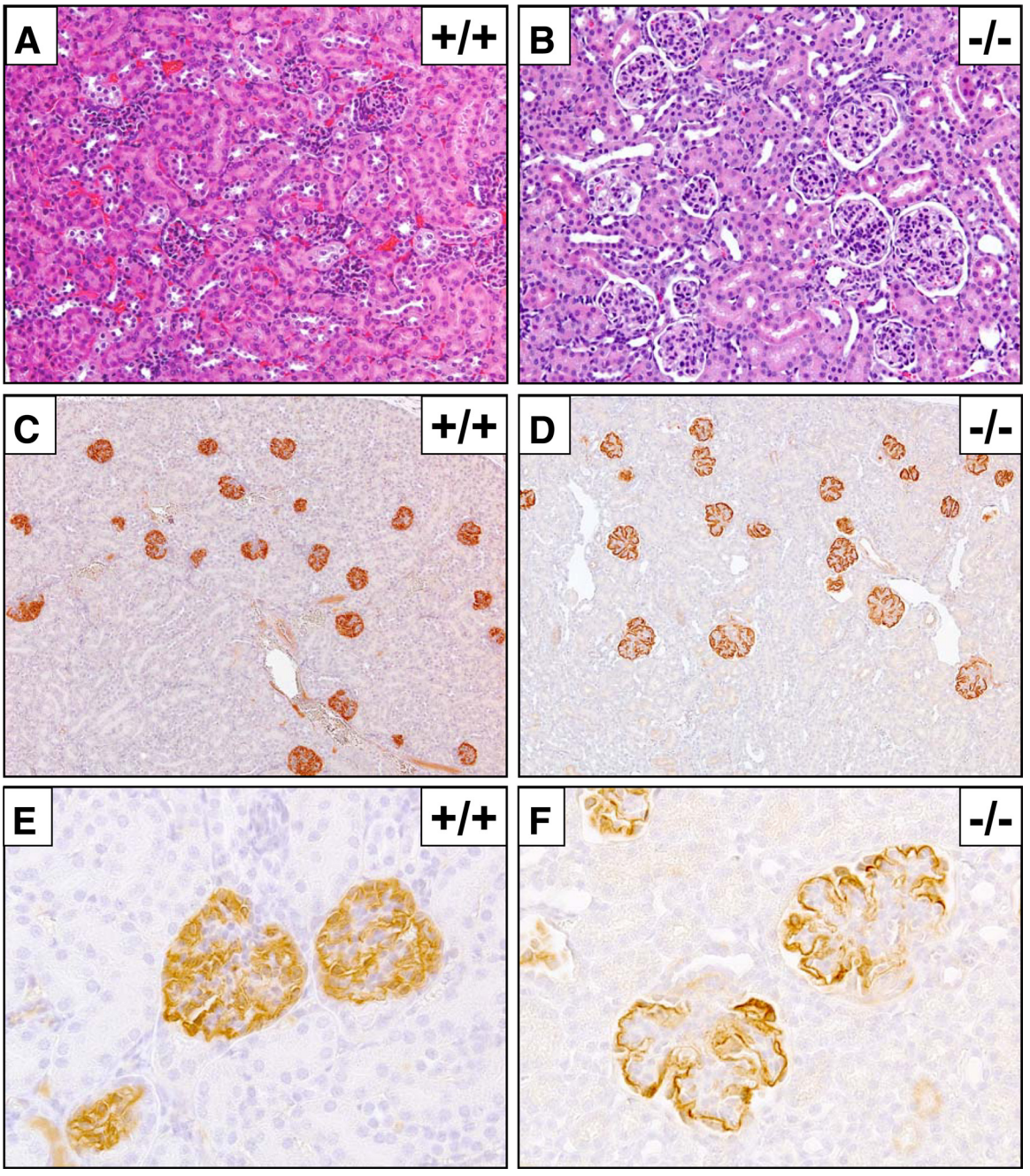

FIG. 3. Glomerular lesions and expression of synaptopodin in 3-week-old *PI3KC2*α-deficient mice. (A and B) Representative H&E-stained kidney sections showing normal glomeruli in WT (+/+) mice (A) and enlarged glomeruli containing increased mesangial tissue in KO (−/−) mice (B). (C to F) Synaptopodin expression in kidney sections from WT (+/+) and KO (−/−) mice. Original magnifications: A and B, ×20; C and D, ×10; E and F, ×40.

glomerulonephropathy in *PI3KC2*$\alpha^{-/-}$ mice consistent with the clinical features and impaired renal function observed in *PI3KC2*α-deficient animals.

PI3KC2α deficiency results in loss of and injury to podocytes. In both WT and KO kidneys, the overall immunohistochemical staining patterns for nephrin were very similar to those seen for synaptopodin. In WT glomeruli at 3 weeks of age, nephrin labeling appeared as linear bands along glomerular basement membranes both centrally and peripherally, and nephrin did not surround the podocyte nucleus. In contrast, nephrin labeling in KO mice was again most intense in the peripheral glomerulus, with only weak and discontinuous staining toward the centers of most glomeruli (Fig. 7A and B). The reduced linear expression of nephrin in KO podocytes at 3 weeks of age was accompanied by strong labeling of the perinuclear cytoplasm. By 4 weeks of age, the overall amount and intensity of nephrin staining in most glomeruli were markedly reduced in KO mice (Fig. 7C and D). Nephrin was almost

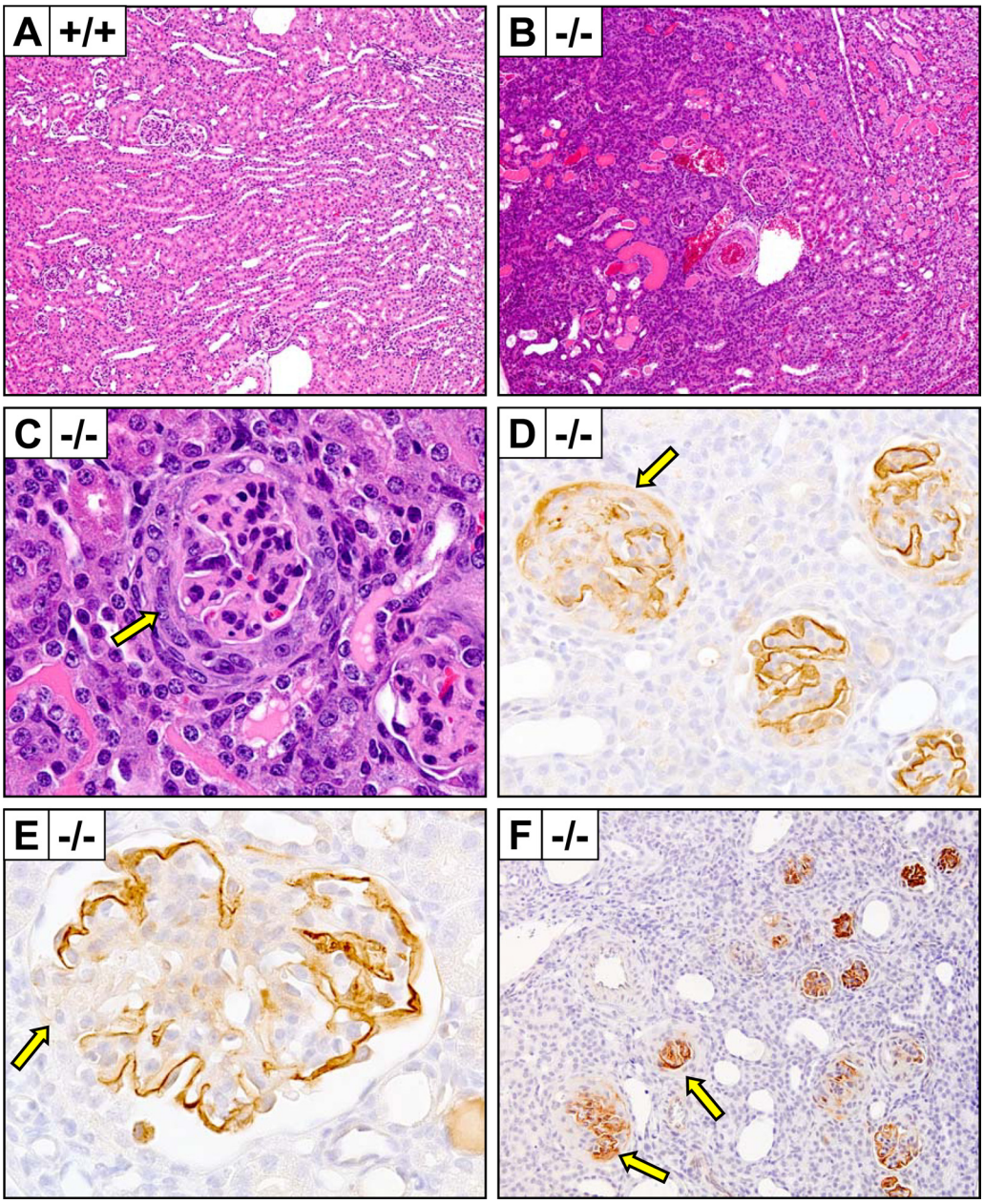

FIG. 4. Glomerular lesions and expression of synaptopodin in 4-week-old *PI3KC2*α-deficient mice. (A to C) Representative H&E-stained kidney sections showing normal glomeruli in WT (+/+) mice (A) and severe renal lesions with widespread tubular dilation, eosinophilic casts, and crescent formation (arrow) in KO (−/−) mice (B and C). (D to F) Synaptopodin expression in kidney sections from KO (−/−) mice, showing reduced expression in areas of crescent formation and sclerosis (arrow in panel D) and absence of expression in areas of adhesions (arrow in panel E). Synaptopodin labeling in the immature subcortical glomeruli (arrows in panel F) was linear and extensive. Original magnifications: A and B, ×10; C, ×60; D, ×20; E, ×60; F, ×20.

absent in areas of glomerulosclerosis and crescent formation and was reduced even in the more normal subcapsular glomeruli. In contrast, by 13 weeks of age in KO mice, although nephrin was virtually absent in sclerotic glomeruli, the intensity and distribution of nephrin labeling were again essentially normal within the remaining functional subcapsular glomeruli (Fig. 7E and F).

In order to determine whether the abnormal staining patterns for synaptopodin and nephrin were associated with reduced numbers of podocytes, kidney sections were stained with the podocyte-specific marker WT-1. Podocyte numbers did not appear to differ markedly between WT and KO mice at 3 weeks of age, although the size of podocyte nuclei in KO kidneys was generally increased (Fig. 8A and B). By 4 weeks of age in KO mice, there were foci where podocytes were absent over glomerular tufts that had formed adhesions to the parietal epithelium, and many of the cells forming the epithelial crescents appeared to be labeled moderately for WT-1, suggesting

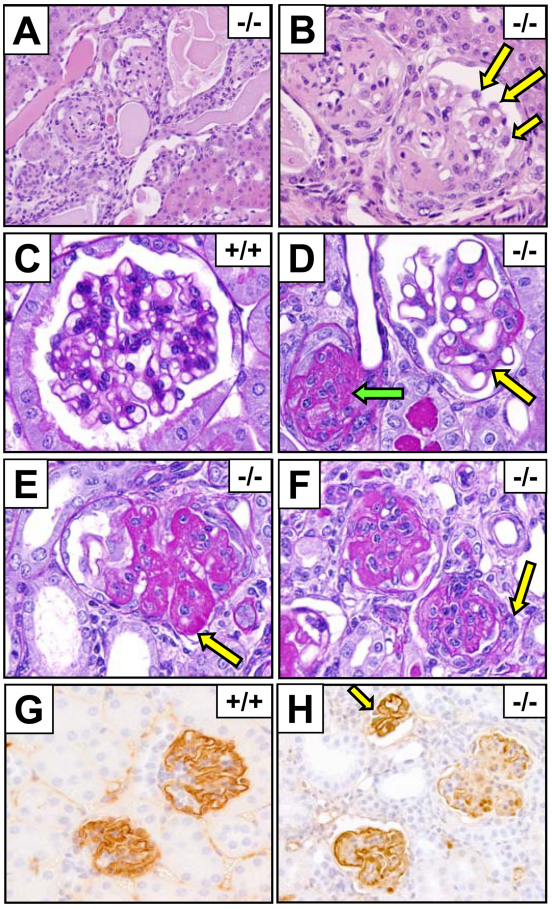

FIG. 5. Glomerular lesions and expression of synaptopodin in 13-week-old *PI3KC2*α-deficient mice. (A and B) Representative glomerular lesions in H&E-stained kidney sections from KO (−/−) mice, showing diffuse mesangial sclerosis. (B) On the left, there is a shrunken nonfunctional sclerotic glomerulus. On the right, there is segmental mesangial sclerosis involving most of the glomerulus; a few patent capillary loops are present, with associated hypertrophic podocytes (arrows). (C to F) PAS-stained kidney sections show normal glomeruli in WT (+/+) mice (C) and glomerular lesions in KO (−/−) mice (D to F) at 13 weeks of age. (D) Lesions varied from relatively mild podocyte hypertrophy and multifocal mesangial thickening (green arrow) to diffuse mesangial sclerosis with ablation of capillaries (yellow arrow). (E and F) Arrows show multilobulated mesangial sclerosis and crescent formation, respectively. (G and H) Synaptopodin expression in kidney sections from WT and KO mice, showing reduced expression in sclerotic juxtaglomerular and cortical glomeruli but linear staining in subcortical glomeruli (arrow). Original magnifications: A, ×20; B, ×40; C to F, ×60; G and H, ×40.

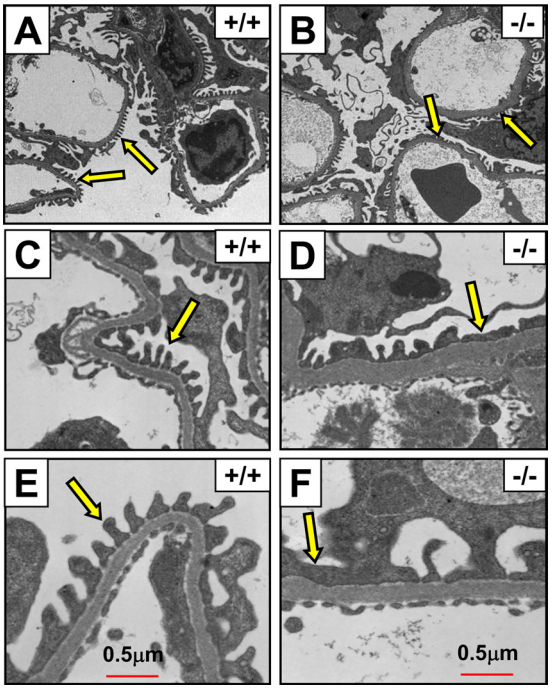

FIG. 6. Ultrastructural analysis of podocyte foot processes in *PI3KC2*α-deficient mice. Representative electron micrographs of kidney sections showing normal and fused podocyte foot processes (arrows) in WT (+/+) and KO (−/−) mice. Original magnifications: A and B, ×3,000; C and D, ×30,000; E and F, ×50,000.

derivation from podocytes or transdifferentiation of another cell type (Fig. 8C and D). At 13 weeks of age, although the number of podocytes in the still-functioning subcapsular glomeruli appeared to be decreased (Fig. 8E and F), podocyte nuclei did not differ markedly in size in comparison to those for WT controls. Podocytes were reduced or absent in many areas with mesangial sclerosis or adhesions, but small numbers of podocytes were still present in apparently nonfunctional glomeruli (Fig. 8G).

To confirm that PI3KC2α deficiency specifically impacts podocytes, kidney sections were stained with desmin, a sensitive marker of podocyte injury and activation (34, 44). Desmin-positive staining in normal WT kidneys in all three age groups was limited to myocytes in muscular arterioles and was entirely absent in glomeruli (data not shown). The distribution of desmin in 3-week-old KO mice was generally similar to that seen in WT controls, being absent in almost all glomeruli. However, desmin was detected in hypertrophic podocytes and mesangial cells in a few glomeruli at 3 weeks of age (Fig. 9A). There was a marked increase in the extent and intensity of desmin-positive cells in most glomeruli in 4-week-old KO mice (Fig. 9B). These desmin-positive cells were located within and around many glomerular crescents (Fig. 9C). In larger crescents, the outermost epithelial cells were most consistently desmin positive, but in many foci the large cells located nearer the glomerular tufts were also labeled. In contrast to the widespread strong staining of glomerular crescents in 4-week-old KO mice, desmin staining in 13-week-old KO mice was minimal to absent in surviving subcapsular glomeruli (Fig. 9D), and only mild positive labeling was detected in sclerotic glomeruli (Fig. 9E). Instead, in 13-week-old KO mice, the most intense and widespread desmin staining was found in interstitial myofibroblasts within those cortical and medullary renal areas showing tubular atrophy and fibrosis (Fig. 9F). Upregulated expression of desmin in kidneys from KO mice was also detected on Western blots (data available on request).

Extensive podocyte loss is accompanied by simultaneous visceral cell hyperplasia in cellular/collapsing FSGS (46). Therefore, we assessed cell proliferation in kidneys by immunohistochemical staining for Ki-67. In 3-week-old mice, there was no detectable difference between WT and KO animals, with Ki-67 generally appearing within individual or paired cells

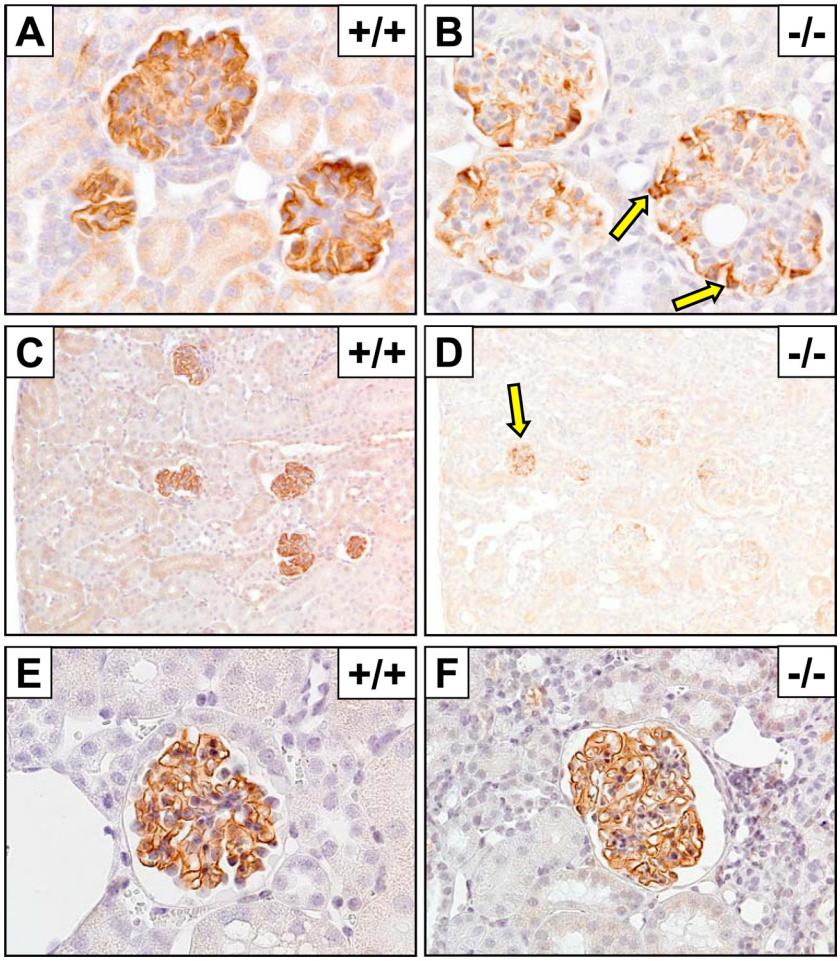

FIG. 7. Glomerular expression of nephrin in *PI3KC2*α-deficient mice. Immunohistochemical staining of nephrin in kidney sections from WT (+/+) and KO (−/−) mice at 3 weeks (A and B), 4 weeks (C and D), and 13 weeks (E and F) of age. Staining shows reduced linear expression in podocytes and strong labeling of the perinuclear cytoplasm (B, arrows) and an absence of nephrin in areas of glomerulosclerosis and crescent formation and reduced expression in the more normal subcapsular glomeruli (D, arrow). Original magnifications: A and B, ×60; C and D, ×20; E, ×60; F, ×40.

of the cortical proximal convoluted tubule epithelium (Fig. 10A and B). In 4-week-old KO mice, the number of Ki-67-positive cells in renal tubules was markedly increased compared to that in WT controls (Fig. 10C and D). Instead of the individual or paired Ki-67-positive cells typically seen in WT kidneys, there were entire segments of tubular epithelium that stained positively (Fig. 10E). In addition, the numerous glomerular crescents in 4-week-old KO mice usually contained positively labeled cells, and some glomerular tufts also contained positively labeled mesangial and surface epithelial cells (Fig. 10F). Very little mitotic activity was detected in 13-week-old WT kidneys; there were very few Ki-67-positive renal tubular epithelial cells and none in glomeruli (Fig. 10G). In contrast, in KO kidneys at 13 weeks of age, Ki-67-positive cells were common in the remaining functional proximal and distal convoluted tubules, although most glomeruli were also devoid of labeled cells (Fig. 10H).

PI3KC2α deficiency results in deposition of IgA and IgG and altered expression of MECA 32 in renal tissue. Deposition of IgA in kidneys is a frequent manifestation in primary chronic glomerulonephritis in humans and in mouse models of IgA nephropathy (5), and in our initial studies on nonperfused kidneys, immunofluorescent staining revealed IgA deposition in the glomeruli of *PI3KC2*$\alpha^{-/-}$ mice (data available on request). We found that the extent and intensity of IgA labeling in renal tissues of both WT and KO mice were markedly reduced with perfusion fixation. In fact, IgA was not detected in either blood vessels or glomeruli in well-perfused areas of WT kidneys at any age, although it was present in adjacent, poorly perfused areas (Fig. 11A). Similarly, IgA was not detected in well-perfused renal tissues in KO mice at 3 weeks of age. Notably, IgA was not detected in the numerous crescents and sclerotic glomeruli in 4-week-old KO mice, even in poorly perfused areas (Fig. 11B). In well-perfused areas of 13-week-old KO kidneys, IgA labeling was faint within the near-normal subcortical glomeruli of KO mice (Fig. 11C). In contrast, granular IgA labeling was widespread and more intense in glomeruli, with diffuse expansion of the mesangial matrix or segmental to diffuse glomerular sclerosis (Fig. 11D). In 13-week-old KO kidneys, granular IgA deposits were present in sclerotic

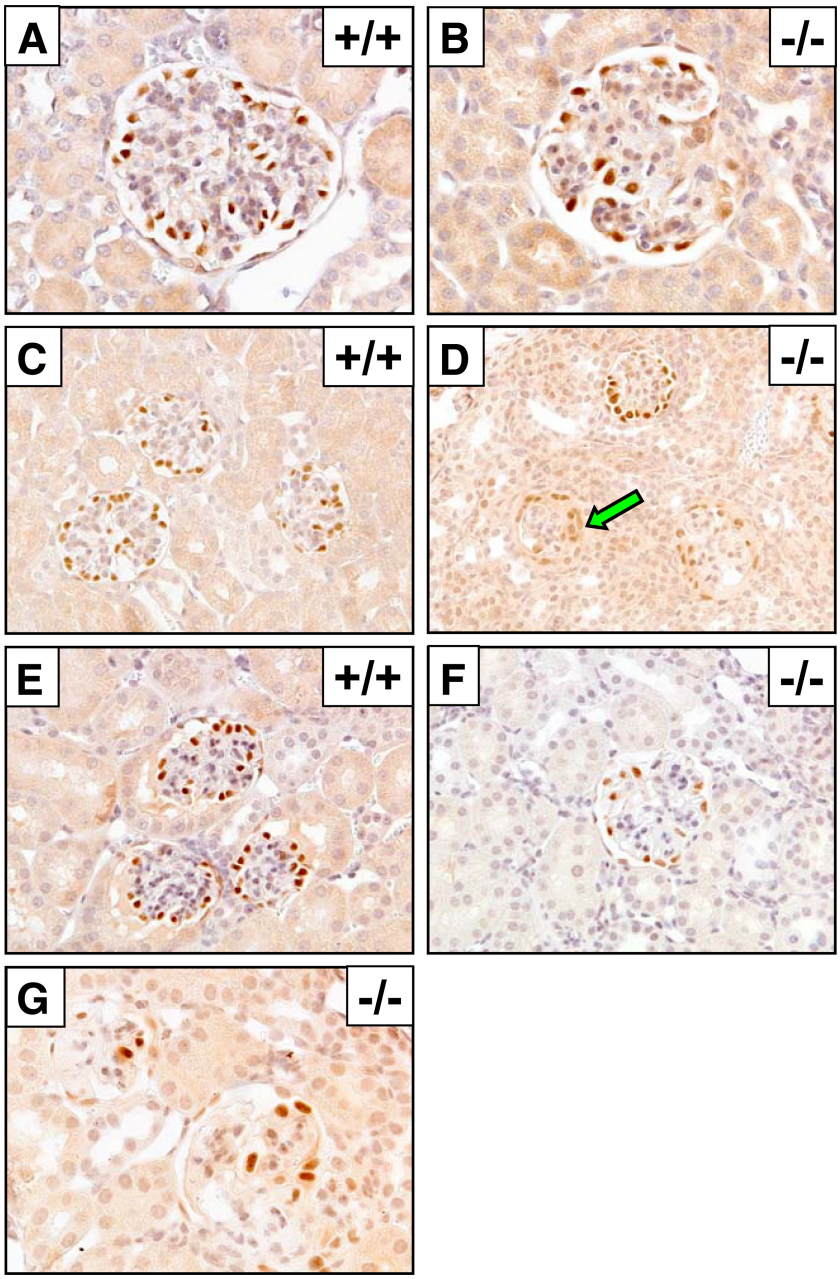

FIG. 8. Glomerular expression of WT-1 in *PI3KC2*α-deficient mice. Immunohistochemical staining of WT-1 in kidney sections from WT (+/+) and KO (−/−) mice at 3 weeks (A and B), 4 weeks (C and D), and 13 weeks (E to G) of age. Staining shows that podocytes were absent over glomerular tufts that had formed adhesions to the parietal epithelium and that many of the cells forming epithelial crescents appear moderately labeled for WT-1 (arrow). Original magnifications: A and B, ×60; C to F, ×40; G, ×60.

glomeruli, but the most intense and consistent IgA staining was present along the brush border of atrophic renal tubules or those containing protein casts (Fig. 11E and F).

Notable differences in distribution of IgG between WT and KO mice were also observed. Well-perfused areas of WT kidneys were essentially devoid of IgG staining at 3 and 4 weeks (Fig. 12A). In contrast, in the kidneys of 3-week-old KO mice, the presence of glomerular leakage was indicated by the intracytoplasmic granular deposits of IgG found within many proximal tubular epithelial cells, as well as within scattered podocytes and mesangial cells (Fig. 12B). By 4 weeks, the extent of IgG staining in the tubular epithelium was reduced considerably, suggesting an overall decrease in glomerular leakage. Interestingly, the most consistently IgG-positive cells at 4 weeks were the basal layers of glomerular crescents, cells that are most likely derived from the parietal epithelium of the proximal tubules (Fig. 12C). At 13 weeks of age, there were generally high levels of background IgG staining present in WT and KO kidneys, but the most intense staining was detected within the cytoplasm and brush border of atrophic proximal

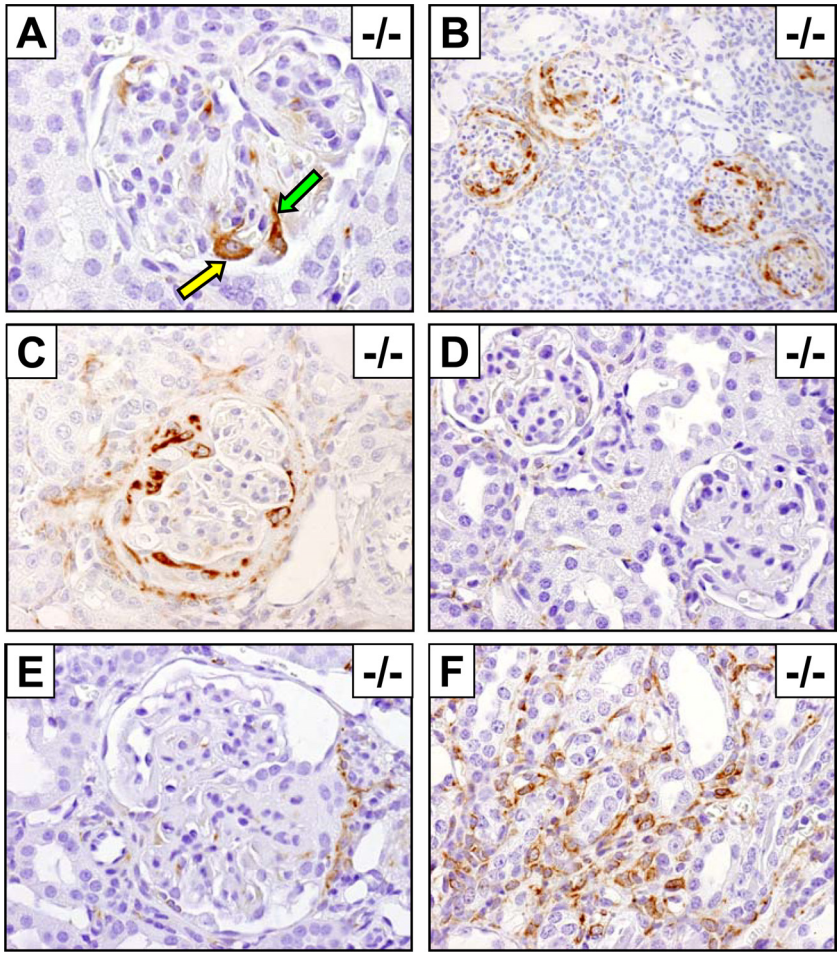

FIG. 9. Expression of desmin in kidneys from *PI3KC2*α-deficient mice. Immunohistochemical staining of desmin in kidney sections from WT (+/+) and KO (−/−) mice at 3 weeks (A and B), 4 weeks (C and D), and 13 weeks (E and F) of age. Staining shows detection of desmin in hypertrophic podocytes (yellow arrow) and mesangial cells (green arrow). Original magnifications: A, ×60; B, ×20; C to F, ×40.

tubules in kidneys from KO mice, accompanied by granular staining within the glomerular mesangium (Fig. 12D).

Altered expression of the pan-endothelial cell marker MECA 32 has previously been observed in the glomeruli of mice that develop renal disease (38). Immunohistochemical staining of perfusion-fixed kidneys from control *PI3KC2*$\alpha^{+/+}$ mice with MECA 32 revealed weakly immunopositive mesangial cells, whereas the tuft endothelium was normally negative. In contrast, the capillary endothelium in KO mice was usually immunopositive for MECA 32 (data available on request).

PI3KC2α-deficient mice have an altered hematological profile but an essentially normal immune response. Since glomerulonephropathies are often associated with changes in immunological parameters, such as serum Ig and autoantibody levels (5), and because other PI3K isoforms affect immune cell activation (19, 30, 40, 47), we paid particular attention to analysis of the immune system of the *PI3KC2*$\alpha^{-/-}$ mice. Splenomegaly (data available on request) and leukocytosis in peripheral blood and spleen (Fig. 13A), affecting all major cell subsets (including $CD4^+$ and $CD8^+$ T cells, B cells, monocytes, and granulocytes), were often observed in *PI3KC2*$\alpha^{-/-}$ mice. Although small yet significant differences were observed in certain thymic and lymph node cell populations, the overall distribution and number of T-cell precursors in the thymus and B-cell maturational stages and granulocytes in the bone marrow (BM), as well as the T- and B-cell content of lymph nodes, were not substantially altered in the *PI3KC2*α-deficient mice (data available on request). The elevated blood leukocyte count in the KO mice was accompanied by significantly increased concentrations of IgA and IgM, autoantibodies, and circulating IgA-fibronectin and immune complexes in the serum (Fig. 13B).

Notwithstanding the observed differences in the cellular and humoral components of the immune system, the *PI3KC2*$\alpha^{-/-}$ mice elicited essentially normal responses in a range of *in vitro* and *in vivo* assays that measure innate and adaptive immune function (data available on request).

***PI3KC2α* deficiency in hematopoietic cells is not sufficient to produce renal disease.** Although *PI3KC2*α deficiency did not have an obvious effect on immune cell activation, it was associated with increased circulating cellular and humoral immune factors, including autoantibodies. This raised the possibility that hematopoietic cells played a role in the development and/or maintenance of renal disease in the *PI3KC2*$\alpha^{-/-}$ mice.

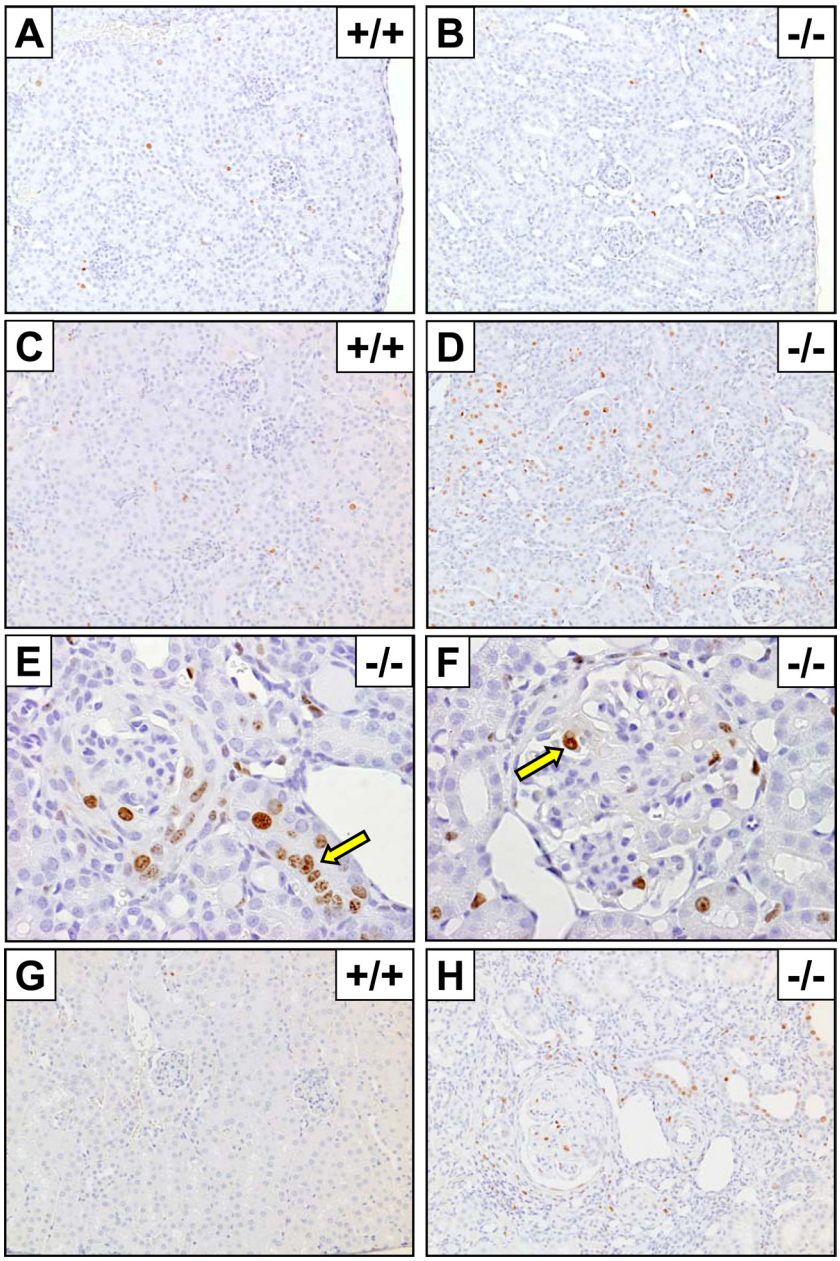

FIG. 10. Expression of Ki-67 in kidneys from *PI3KC2*α-deficient mice. Immunohistochemical staining of Ki-67 in kidney sections from WT (+/+) and KO (−/−) mice at 3 weeks (A and B), 4 weeks (C to F), and 13 weeks (G and H) of age. Staining shows Ki-67-positive epithelial cells (E, arrow) and positively labeled mesangial and surface epithelial cells (F, arrow). Original magnifications: A to D, G, and H, ×20; E and F, ×40.

To test this hypothesis, we used *PI3KC2*α KO and WT mice to generate reciprocal groups of BM chimeras by transplanting KO BM into WT hosts and vice versa and monitored renal function and pathology in both cohorts. When WT mice were assessed at 16 to 20 weeks after transplantation with KO BM, they did not exhibit an abnormal clinical profile either in blood chemistry or in cellular and humoral immune parameters, and they did not show glomerular lesions. On the other hand, the abnormal clinical parameters and glomerulosclerosis were still present in *PI3KC2*$\alpha^{-/-}$ mice after reconstitution of BM with WT cells (Fig. 14). In summary, data from these studies demonstrated that expression of PI3KC2α in nonhematopoietic cells, presumably in the kidney itself, is critical for normal renal function.

DISCUSSION

PI3KC2α is critical for normal renal function. The function of PI3K enzymes as downstream effectors in signal transduction pathways, particularly in the immune system and in cancer development, has been well established over the past years (19, 27, 30, 40, 47, 51). However, knowledge of the isoform-specific role of PI3K variants, especially in the class II family, remains limited. In this study we demonstrate that, unlike other studied

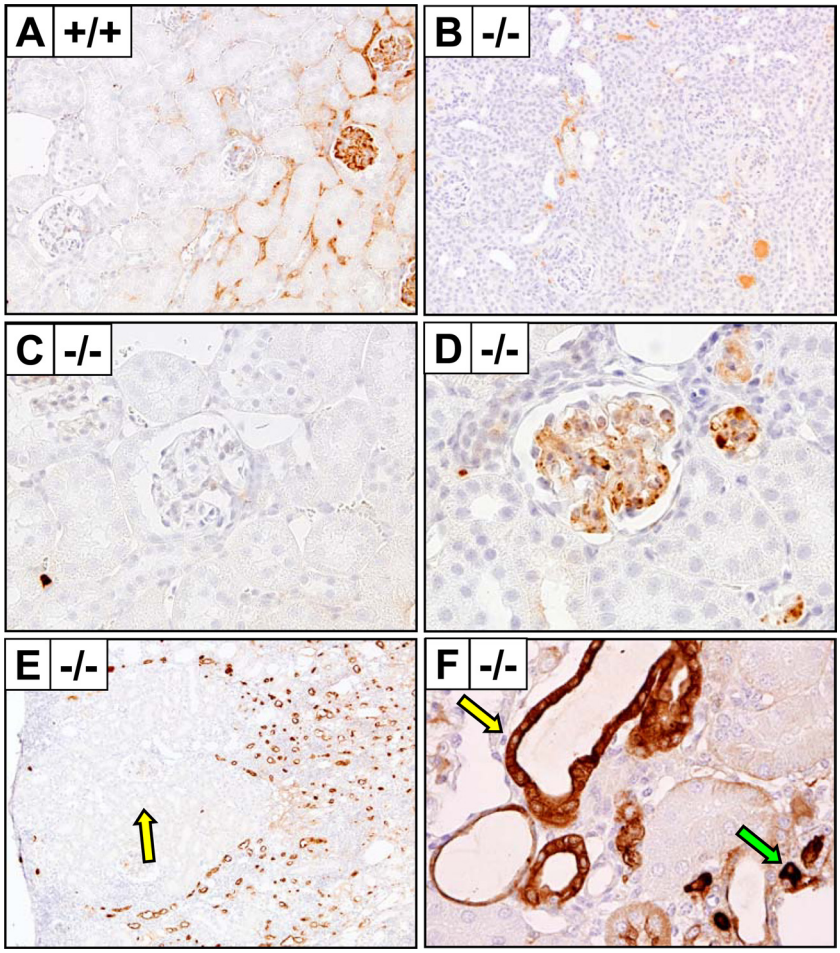

FIG. 11. Deposition of IgA in kidneys from *PI3KC2*α-deficient mice. Immunohistochemical staining of IgA in kidney sections from WT (+/+) and KO (−/−) mice. (A) IgA is detected only in poorly perfused areas in kidneys from 13-week-old WT mice. (B) IgA is not detected in kidneys from 4-week-old KO mice, even in poorly perfused areas. (C and D) In well-perfused areas of kidneys from 13-week-old KO mice, IgA staining is faint within normal subcortical glomeruli (C) but is widespread in glomeruli with diffuse expansion of the mesangial matrix (D). (E and F) The most intense staining for IgA is along the brush border of atrophic renal tubules. (E) The arrow denotes the near absence of IgA in the surviving near-normal cortical tubules and glomeruli. (F) Positive staining of the renal tubular epithelium (yellow arrow) and plasma cells in the interstitial tissue (green arrow). Original magnifications: A and B, ×20; C and D, ×40; E, ×10; F, ×60.

PI3K isoforms, PI3KC2α is not intrinsic to immune cell development and function but is essential for maintenance of normal renal homeostasis. *PI3KC2*α deficiency in mice led to characteristic clinical manifestations of chronic kidney disease: failure to thrive, elevated serum creatinine and BUN levels, decreased creatinine clearance, increased IgA response, and a range of histopathological lesions consistent with glomerulonephropathy. *PI3KC2*$\alpha^{-/-}$ mice presented relatively mild proteinuria, which was unexpected in the face of diffuse severe glomerulonephropathy and effacement of podocyte foot processes; yet, a similar lack of correlation between the extent of podocyte damage and the degree of proteinuria has been observed previously in humans (48). The renal parenchyma in *PI3KC2*$\alpha^{-/-}$ mice was markedly reduced in volume and characterized by areas of widespread atrophy. Of note, many renal tubules of *PI3KC2*$\alpha^{-/-}$ animals were filled with eosinophilic proteinaceous fluid and showed evidence of an aberrant hyperplastic response manifesting in microcystic transformation. Normally, control of renal epithelial proliferation and tubule diameter is dependent on detection of adequate urine flow by mechanosensory primary cilia. Together, these findings are consistent with the hypothesis that lack of urine flow due to loss of capillaries in sclerotic glomeruli could be responsible for the milder-than-expected protein excretion in the urine.

Development of renal lesions appears to be accelerated during weaning (4 weeks of age). At this point, it is not possible to say if the stress, dietary changes, or rapid growth that normally occurs at this age in mice is responsible for the onset of glomerular lesions. However, regardless of the cause, it appears that the nonfunctional immature subcapsular glomeruli that are present in 4-week-old mice are mostly spared and that these glomeruli may be largely responsible for the long-term survival of the majority of KO mice. Thus, PI3KC2α deficiency is associated with an acute severe glomerulopathy coincident with weaning, followed by a slowly progressive glomerulonephropathy with features traditionally associated with IgA nephropathy in older mice.

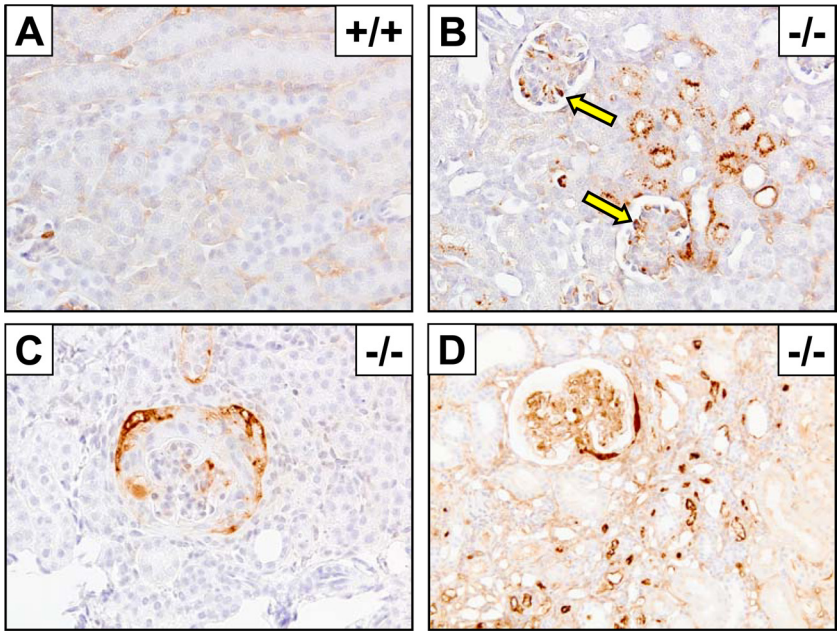

FIG. 12. Deposition of IgG in kidneys from *PI3KC2*α-deficient mice. Immunohistochemical staining of IgG in kidney sections from WT (+/+) and KO (−/−) mice. (A and B) In 3-week-old mice, IgG is absent in well-perfused areas of WT kidneys but present in many proximal tubular epithelial cells and in some scattered podocytes and mesangial cells (arrows) in kidneys from KO mice. (C) IgG staining in glomerular crescents in kidneys from 4-week-old KO mice. (D) IgG staining is most intense in the brush border of atrophic tubules in kidneys from 13-week-old KO mice. Original magnifications: A, ×40; B to D, ×20.

What is the role of the immune system in the development of glomerulonephritis during *PI3KC2*α deficiency? The contribution of the immune system to the initiation and progression of glomerular diseases, including IgA nephropathy, remains unclear. No animal model of glomerulonephritis in which transplantation of BM from a diseased donor recapitulated the disease in a syngeneic host has been published to date. However, in humans, the disease often recurs in the healthy donor kidney after renal transplantation, which implicates extrarenal components in the development of certain types of glomerulonephritis (24). It is possible that interplay between the immune system and processes inherent to the kidney governs the rate of disease progression in glomerulonephritis. For instance, it has been suggested recently that clearance of Ab and immune complexes could be part of normal podocyte function and that the damage inflicted by the immune system may be amplified in the presence of podocyte dysfunction (1). In this regard, it is of particular interest that in *PI3KC2*α-deficient mice, podocyte alterations are apparent even before IgA is present in significant amounts (at 3 weeks). The severe lesions that develop at 4 weeks of age also appear independent of IgA deposition. Thus, in the case of PI3KC2α deficiency, the presence of IgA does not appear to play a major role in the pathogenesis of renal damage in young (3- to 4-week-old) KO mice. This is an important finding and contrasts with the widely held belief that IgA is a required factor in the pathogenesis of IgA nephropathy (17, 32). Moreover, although levels of IgA were elevated in serum and kidney tissue in older KO mice, the nephropathy in these animals is most likely a consequence of the acute damage suffered at weaning and not directly mediated by or dependent on the presence of IgA.

Even though one of the most studied aspects of PI3K pathways is related to immune function, cells of hematopoietic origin were not sufficient to elicit glomerulonephropathy in mice transplanted with *PI3KC2*α-deficient BM. In addition, the *in vivo* and *in vitro* functionality of immune cells from *PI3KC2*$\alpha^{-/-}$ mice was not significantly impaired. Nevertheless, the mutant mice showed signs of leukocytosis and anemia, as well as increased levels of serum IgA, IgM, and immune complexes, parameters which are frequently associated with primary chronic glomerulonephritis. Together, these results indicate that the kidney disease of the *PI3KC2*$\alpha^{-/-}$ mice is not induced by inherent immune-mediated processes but rather is due to an intrinsic glomerular defect(s).

How can the PI3KC2α pathway contribute to kidney function? A full-length PI3KC2α protein was clearly absent in the mutant mice, with a concomitant profound decrease in enzyme activity, which indicates that normal renal function is sensitive to reduction in the level of PI3KC2α activity. Yet, a weakly expressed truncated protein, lacking the tandem C-terminal PX and C2 domains, was detected in *PI3KC2*$\alpha^{-/-}$ mice, which raises the possibility that these domains play a particularly critical role in glomerular function. The subcellular localization of PI3KC2α is thought to be an important factor regulating the spatial and temporal production of 3-phosphoinositides in different cellular compartments. Localization of PI3KC2α in clathrin-coated vesicles and the TGN appears to be independent of the PX and C2 domains, however, since full-length PI3KC2α and deletion mutants lacking the PX and/or C2 domain display similar patterns of cytoplasmic distribution (12). A nuclear localization sequence, present in the C2 domain, facilitates translocation of PI3KC2α to the nucleus, where it

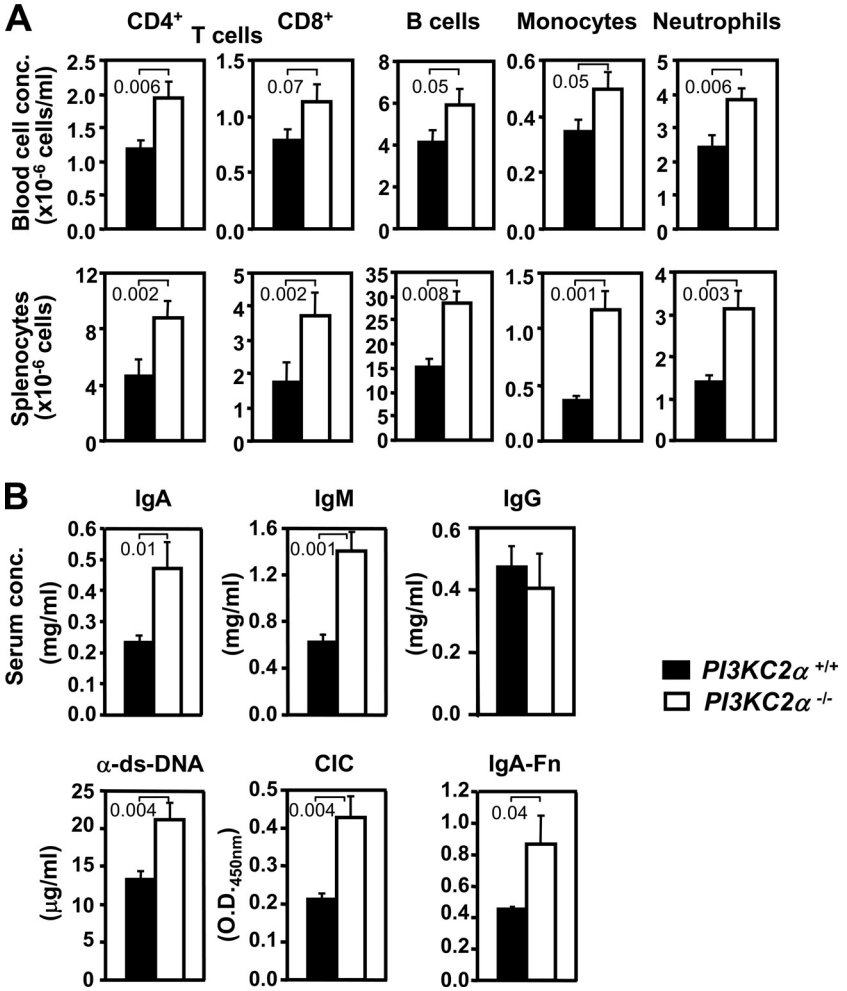

FIG. 13. Chronic glomerular disease in *PI3KC2*$\alpha^{-/-}$ mice is accompanied by leukocytosis and elevated concentration of humoral immune parameters. (A) Hematopoietic cell profiles in blood and spleen of mice with the indicated genotypes at 8 weeks of age. (B) The indicated serum parameters were measured at 8 to 24 weeks of age. Data from 8 to 19 mice per cohort were pooled from 2 to 4 independent experiments giving similar results. Numbers above the bars indicate *P* values compared to results for the WT. ds-DNA, double-stranded DNA; CIC, circulating immune complex; IgA-Fn, IgA-fibronectin.

localizes in nuclear speckles (11). Since PI3KC2α mutant protein does not express this sequence, we anticipate that it is retained in a cytoplasmic compartment. Importantly, the two class II isoforms, C2α and C2β, possess homologous PX and C2 domains and also share widespread tissue expression (16) and common signaling pathways (4). Despite these similarities, it is apparent that the functions of these closely related isoforms are not redundant, since *PI3KC2*β-null mice are reported to be viable and fertile and display no apparent histological abnormalities (22). It is important to note that, according to one report, deletion of the C2 domain from PI3KC2β increased its catalytic activity (3). We could not confirm such an effect of the mutation on PI3KC2α activity, since *PI3KC2*$\alpha^{-/-}$ tissues registered significantly decreased PI3KC2α activity and contained very low levels of the truncated enzyme, possibly reflecting the inherent instability of the truncated protein.

PI3K2α-deficient mice exhibited alterations in podocyte morphology and number. Podocytes perform a critical role in the glomerular filtration process, forming the slit diaphragm, a size- and charge-selective filtration barrier which limits protein leakage (42). A number of genes that regulate glomerular structures and function have been identified (6, 9, 14, 25, 28, 29, 43). We and others have shown that inactivating mutations of genes, such as *nephrin* (28), *podocin* (6), *CD2-associated protein* (*CD2AP*) (43), *Neph1* (14), *Nck* (25), *alpha-actinin-4* (29), and *mFAT1* (9), typically result in the development of nephrotic syndrome with effacement of podocyte foot processes. One of the few slit diaphragm signaling pathways that has been studied in detail is the transmembrane signaling protein nephrin, which interacts with podocin and the adaptor protein CD2AP, resulting in AKT activation (36). Both nephrin and CD2AP have been shown to affect podocyte morphology and function via their association with PI3K, inducing PI3K-p85/AKT-mediated signaling (23, 54). Altered modulation of PI3K/AKT pathways in IgA nephropathy has recently been reported (10). Regulation of actin filaments in foot processes is important for maintaining integrity of the cytoskeleton and functionality of the slit diaphragm. Nephrin-mediated

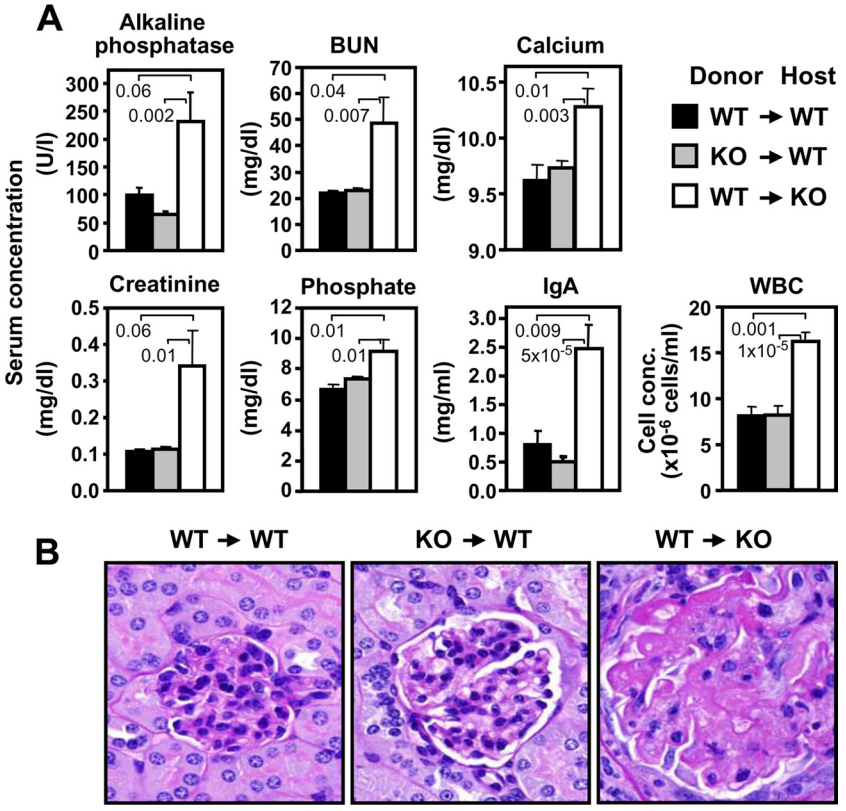

FIG. 14. Development of renal disease in *PI3KC2*$\alpha^{-/-}$ mice is regulated by cells of nonhematopoietic origin. (A) BM chimeric mice as designated were assessed for the indicated blood parameters 16 to 20 weeks after BM reconstitution. Numbers above the bars indicate *P* values compared to results for the WT. WBC, white blood cells. (B) Representative PAS staining of kidney sections 20 weeks after BM transplantation shows normal glomeruli in WT host mice regardless of the genotype of the donor BM. In contrast, glomerular lesions, characterized by diffuse glomerulosclerosis, with increased mesangium, glomerular capillary collapse, and effacement, are evident in KO mice who received WT BM. Data were obtained using 8 to 11 mice per cohort and are representative of 2 independent experiments.

activation of both AKT and Rac 1 has been shown to induce changes in cytoskeleton remodeling in cultured rat podocytes and is dependent upon the activity of PI3K (54). Importantly, these effects were dependent on nephrin overexpression in cultured cells, and it is possible that other PI3K isoforms may be involved in regulation of cytoskeleton signaling in podocytes under physiological conditions *in vivo*. Another potential mechanism of podocyte injury in the absence of PI3K activity is increased sensitivity of podocytes to apoptosis (41). Selective engagement of PI3K-p85 by nephrin and CD2AP is known to promote phosphorylation of AKT, which serves as a potent antiapoptotic regulator protecting podocytes from cell death (23). Similarly, inhibition of PI3KC2α expression is associated with increased susceptibility to apoptosis and decreased proliferative capacity in various cell types (15, 35). Increased expression of the proapoptotic cytokine transforming growth factor β (TGF-β) has been observed in CD2AP-deficient mice (41). Podocytes from these mice showed enhanced susceptibility to apoptosis, whereas WT podocytes were protected from TGF-β-induced apoptosis by enhanced PI3K/AKT and ERK1/2 signaling in a CD2AP-dependent manner (41). While we have not looked within glomerular tissue, serum TGF-β levels were not elevated in PI3KC2α mutant mice (data available on request). In addition, terminal deoxynucleotidyltransferase-mediated dUTP-biotin nick end labeling (TUNEL) staining of kidney samples from 13-week-old WT and KO mice for apoptotic cells showed only rare positive signals in degenerate glomerular tufts and epithelial cells (data available on request). It is important to note that besides its role in podocyte apoptosis, the PI3K/Akt signaling pathway was implicated in the control of renal epithelial cell proliferation (52). Besides loss of podocytes, visceral cell hyperplasia is another pathological feature of cellular/collapsing FSGS, and the number of epithelial cells labeled with the proliferation marker Ki-67 was markedly increased in the kidneys of *PI3K2*α-deficient mice. The sequence of biochemical and cellular interactions that regulate epithelial cell proliferation and podocyte survival is poorly defined; therefore, further investigation is required to establish the place of PI3K2α in these complex processes.

Given the expression pattern of PI3KC2α in the kidney and the fact that *PI3KC2*$\alpha^{-/-}$ mice display many of the glomerular lesions associated with podocyte injury, it is likely that this isoform, like PI3K-p85, plays a role in the signaling cascade regulating podocyte development and/or survival. It is possible that this kinase has pleotrophic effects, which include the differentiation and maintenance of podocytes as well as perhaps the modulation of IgA production. Future studies using PI3KC2α-deficient podocytes and renal epithelial cells will help to determine the precise molecular interactions involved

in PI3KC2α signaling cascades and facilitate identification of factors involved in the pathological mechanisms leading to the multifaceted features of progressive glomerulonephritis.

ACKNOWLEDGMENTS

We are grateful to Larry Rodriguez for help with statistical analysis and to Amin Al Shami, Kathy Henze, Mary Thiel, Ryan Vance, James Syrewicz, and June Wingert for expert technical assistance in performing histological procedures.

REFERENCES

1. **Akilesh, S., T. B. Huber, H. Wu, G. Wang, B. Hartleben, J. B. Kopp, J. H. Miner, D. C. Roopenian, E. R. Unanue, and A. S. Shaw.** 2008. Podocytes use FcRn to clear IgG from the glomerular basement membrane. Proc. Natl. Acad. Sci. U. S. A. **105:**967–972.
2. **Anderson, S. J., J. P. Lauritsen, M. G. Hartman, A. M. Foushee, J. M. Lefebvre, S. A. Shinton, B. Gerhardt, R. R. Hardy, T. Oravecz, and D. L. Wiest.** 2007. Ablation of ribosomal protein L22 selectively impairs alphabeta T cell development by activation of a p53-dependent checkpoint. Immunity **26:**759–772.
3. **Arcaro, A., S. Volinia, M. J. Zvelebil, R. Stein, S. J. Watton, M. J. Layton, I. Gout, K. Ahmadi, J. Downward, and M. D. Waterfield.** 1998. Human phosphoinositide 3-kinase C2beta, the role of calcium and the C2 domain in enzyme activity. J. Biol. Chem. **273:**33082–33090.
4. **Arcaro, A., M. J. Zvelebil, C. Wallasch, A. Ullrich, M. D. Waterfield, and J. Domin.** 2000. Class II phosphoinositide 3-kinases are downstream targets of activated polypeptide growth factor receptors. Mol. Cell. Biol. **20:**3817–3830.
5. **Barratt, J., A. C. Smith, K. Molyneux, and J. Feehally.** 2007. Immunopathogenesis of IgAN. Semin. Immunopathol. **29:**427–443.
6. **Boute, N., O. Gribouval, S. Roselli, F. Benessy, H. Lee, A. Fuchshuber, K. Dahan, M. C. Gubler, P. Niaudet, and C. Antignac.** 2000. NPHS2, encoding the glomerular protein podocin, is mutated in autosomal recessive steroid-resistant nephrotic syndrome. Nat. Genet. **24:**349–354.
7. **Brommage, R., U. Desai, J. P. Revelli, D. B. Donoviel, G. K. Fontenot, C. M. Dacosta, D. D. Smith, L. L. Kirkpatrick, K. J. Coker, M. S. Donoviel, D. E. Eberhart, K. H. Holt, M. R. Kelly, W. J. Paradee, A. V. Philips, K. A. Platt, A. Suwanichkul, G. M. Hansen, A. T. Sands, B. P. Zambrowicz, and D. R. Powell.** 2008. High-throughput screening of mouse knockout lines identifies true lean and obese phenotypes. Obesity (Silver Spring) **16:**2362–2367.
8. **Brown, R. A., J. Domin, A. Arcaro, M. D. Waterfield, and P. R. Shepherd.** 1999. Insulin activates the alpha isoform of class II phosphoinositide 3-kinase. J. Biol. Chem. **274:**14529–14532.
9. **Ciani, L., A. Patel, N. D. Allen, and C. ffrench-Constant.** 2003. Mice lacking the giant protocadherin mFAT1 exhibit renal slit junction abnormalities and a partially penetrant cyclopia and anophthalmia phenotype. Mol. Cell. Biol. **23:**3575–3582.
10. **Cox, S. N., F. Sallustio, G. Serino, P. Pontrelli, R. Verrienti, F. Pesce, D. D. Torres, N. Ancona, P. Stifanelli, G. Zaza, and F. P. Schena.** 2010. Altered modulation of WNT-beta-catenin and PI3K/Akt pathways in IgA nephropathy. Kidney Int. **78:**396–407.
11. **Didichenko, S. A., and M. Thelen.** 2001. Phosphatidylinositol 3-kinase c2alpha contains a nuclear localization sequence and associates with nuclear speckles. J. Biol. Chem. **276:**48135–48142.
12. **Domin, J., I. Gaidarov, M. E. Smith, J. H. Keen, and M. D. Waterfield.** 2000. The class II phosphoinositide 3-kinase PI3K-C2alpha is concentrated in the trans-Golgi network and present in clathrin-coated vesicles. J. Biol. Chem. **275:**11943–11950.
13. **Domin, J., F. Pages, S. Volinia, S. E. Rittenhouse, M. J. Zvelebil, R. C. Stein, and M. D. Waterfield.** 1997. Cloning of a human phosphoinositide 3-kinase with a C2 domain that displays reduced sensitivity to the inhibitor wortmannin. Biochem. J. **326:**139–147.
14. **Donoviel, D. B., D. D. Freed, H. Vogel, D. G. Potter, E. Hawkins, J. P. Barrish, B. N. Mathur, C. A. Turner, R. Geske, C. A. Montgomery, M. Starbuck, M. Brandt, A. Gupta, R. Ramirez-Solis, B. P. Zambrowicz, and D. R. Powell.** 2001. Proteinuria and perinatal lethality in mice lacking NEPH1, a novel protein with homology to NEPHRIN. Mol. Cell. Biol. **21:**4829–4836.
15. **Elis, W., E. Triantafellow, N. M. Wolters, K. R. Sian, G. Caponigro, J. Borawski, L. A. Gaither, L. O. Murphy, P. M. Finan, and J. P. Mackeigan.** 2008. Down-regulation of class II phosphoinositide 3-kinase alpha expression below a critical threshold induces apoptotic cell death. Mol. Cancer Res. **6:**614–623.
16. **El Sheikh, S. S., J. Domin, P. Tomtitchong, P. Abel, G. Stamp, and E. N. Lalani.** 2003. Topographical expression of class IA and class II phosphoinositide 3-kinase enzymes in normal human tissues is consistent with a role in differentiation. BMC Clin. Pathol. **3:**4.
17. **Endo, Y.** 1997. IgA nephropathy—human disease and animal model. Ren. Fail. **19:**347–371.
18. **Falasca, M., W. E. Hughes, V. Dominguez, G. Sala, F. Fostira, M. Q. Fang, R. Cazzolli, P. R. Shepherd, D. E. James, and T. Maffucci.** 2007. The role of phosphoinositide 3-kinase C2alpha in insulin signaling. J. Biol. Chem. **282:**28226–28236.
19. **Fruman, D. A., and G. Bismuth.** 2009. Fine tuning the immune response with PI3K. Immunol. Rev. **228:**253–272.
20. **Gaidarov, I., M. E. Smith, J. Domin, and J. H. Keen.** 2001. The class II phosphoinositide 3-kinase C2alpha is activated by clathrin and regulates clathrin-mediated membrane trafficking. Mol. Cell **7:**443–449.
21. **Gaidarov, I., Y. Zhao, and J. H. Keen.** 2005. Individual phosphoinositide 3-kinase C2alpha domain activities independently regulate clathrin function. J. Biol. Chem. **280:**40766–40772.
22. **Harada, K., A. B. Truong, T. Cai, and P. A. Khavari.** 2005. The class II phosphoinositide 3-kinase C2beta is not essential for epidermal differentiation. Mol. Cell. Biol. **25:**11122–11130.
23. **Huber, T. B., B. Hartleben, J. Kim, M. Schmidts, B. Schermer, A. Keil, L. Egger, R. L. Lecha, C. Borner, H. Pavenstadt, A. S. Shaw, G. Walz, and T. Benzing.** 2003. Nephrin and CD2AP associate with phosphoinositide 3-OH kinase and stimulate AKT-dependent signaling. Mol. Cell. Biol. **23:**4917–4928.
24. **Ivanyi, B.** 2008. A primer on recurrent and de novo glomerulonephritis in renal allografts. Nat. Clin. Pract. Nephrol. **4:**446–457.
25. **Jones, N., I. M. Blasutig, V. Eremina, J. M. Ruston, F. Bladt, H. Li, H. Huang, L. Larose, S. S. Li, T. Takano, S. E. Quaggin, and T. Pawson.** 2006. Nck adaptor proteins link nephrin to the actin cytoskeleton of kidney podocytes. Nature **440:**818–823.
26. **Kang, S., J. Song, J. Kang, H. Kang, D. Lee, Y. Lee, and D. Park.** 2005. Suppression of the alpha-isoform of class II phosphoinositide 3-kinase gene expression leads to apoptotic cell death. Biochem. Biophys. Res. Commun. **329:**6–10.
27. **Katso, R., K. Okkenhaug, K. Ahmadi, S. White, J. Timms, and M. D. Waterfield.** 2001. Cellular function of phosphoinositide 3-kinases: implications for development, homeostasis, and cancer. Annu. Rev. Cell Dev. Biol. **17:**615–675.
28. **Kestila, M., U. Lenkkeri, M. Mannikko, J. Lamerdin, P. McCready, H. Putaala, V. Ruotsalainen, T. Morita, M. Nissinen, R. Herva, C. E. Kashtan, L. Peltonen, C. Holmberg, A. Olsen, and K. Tryggvason.** 1998. Positionally cloned gene for a novel glomerular protein—nephrin—is mutated in congenital nephrotic syndrome. Mol. Cell **1:**575–582.
29. **Kos, C. H., T. C. Le, S. Sinha, J. M. Henderson, S. H. Kim, H. Sugimoto, R. Kalluri, R. E. Gerszten, and M. R. Pollak.** 2003. Mice deficient in alpha-actinin-4 have severe glomerular disease. J. Clin. Invest. **111:**1683–1690.
30. **Ktori, C., P. R. Shepherd, and L. O'Rourke.** 2003. TNF-alpha and leptin activate the alpha-isoform of class II phosphoinositide 3-kinase. Biochem. Biophys. Res. Commun. **306:**139–143.
31. **Marone, R., V. Cmiljanovic, B. Giese, and M. P. Wymann.** 2008. Targeting phosphoinositide 3-kinase: moving towards therapy. Biochim. Biophys. Acta **1784:**159–185.
32. **Miyawaki, S., E. Muso, E. Takeuchi, H. Matsushima, Y. Shibata, S. Sasayama, and H. Yoshida.** 1997. Selective breeding for high serum IgA levels from noninbred ddY mice: isolation of a strain with an early onset of glomerular IgA deposition. Nephron **76:**201–207.
33. **Molz, L., Y. W. Chen, M. Hirano, and L. T. Williams.** 1996. Cpk is a novel class of Drosophila PtdIns 3-kinase containing a C2 domain. J. Biol. Chem. **271:**13892–13899.
34. **Nagase, M., S. Shibata, S. Yoshida, T. Nagase, T. Gotoda, and T. Fujita.** 2006. Podocyte injury underlies the glomerulopathy of Dahl salt-hypertensive rats and is reversed by aldosterone blocker. Hypertension **47:**1084–1093.

34a. **National Research Council.** 1996. Guide for the care and use of laboratory animals. National Academy Press, Washington, DC.

35. **Ng, S. K., S. Y. Neo, Y. W. Yap, R. K. Karuturi, E. S. Loh, K. H. Liau, and E. C. Ren.** 2009. Ablation of phosphoinositide-3-kinase class II alpha suppresses hepatoma cell proliferation. Biochem. Biophys. Res. Commun. **387:**310–315.
36. **Patrakka, J., and K. Tryggvason.** 2007. Nephrin—a unique structural and signaling protein of the kidney filter. Trends Mol. Med. **13:**396–403.
37. **Paulhe, F., B. Perret, H. Chap, N. Iberg, O. Morand, and C. Racaud-Sultan.** 2002. Phosphoinositide 3-kinase C2alpha is activated upon smooth muscle cell migration and regulated by alpha (v) beta(3) integrin engagement. Biochem. Biophys. Res. Commun. **297:**261–266.
38. **Powell, D. R., U. Desai, M. J. Sparks, G. Hansen, J. Gay, J. Schrick, Z. Z. Shi, J. Hicks, and P. Vogel.** 2005. Rapid development of glomerular injury and renal failure in mice lacking p53R2. Pediatr. Nephrol. **20:**432–440.
39. **Prior, I. A., and M. J. Clague.** 1999. Localization of a class II phosphatidylinositol 3-kinase, PI3KC2alpha, to clathrin-coated vesicles. Mol. Cell. Biol. Res. Commun. **1:**162–166.
40. **Rommel, C., M. Camps, and H. Ji.** 2007. PI3K delta and PI3K gamma: partners in crime in inflammation in rheumatoid arthritis and beyond? Nat. Rev. Immunol. **7:**191–201.
41. **Schiffer, M., P. Mundel, A. S. Shaw, and E. P. Bottinger.** 2004. A novel role for the adaptor molecule CD2-associated protein in transforming growth factor-beta-induced apoptosis. J. Biol. Chem. **279:**37004–37012.

42. **Shankland, S. J.** 2006. The podocyte's response to injury: role in proteinuria and glomerulosclerosis. Kidney Int. **69:**2131–2147.
43. **Shih, N. Y., J. Li, V. Karpitskii, A. Nguyen, M. L. Dustin, O. Kanagawa, J. H. Miner, and A. S. Shaw.** 1999. Congenital nephrotic syndrome in mice lacking CD2-associated protein. Science **286:**312–315.
44. **Smeets, B., N. A. Te Loeke, H. B. Dijkman, M. L. Steenbergen, J. F. Lensen, M. P. Begieneman, T. H. van Kuppevelt, J. F. Wetzels, and E. J. Steenbergen.** 2004. The parietal epithelial cell: a key player in the pathogenesis of focal segmental glomerulosclerosis in Thy-1.1 transgenic mice. J. Am. Soc. Nephrol. **15:**928–939.
45. **Stahelin, R. V., D. Karathanassis, K. S. Bruzik, M. D. Waterfield, J. Bravo, R. L. Williams, and W. Cho.** 2006. Structural and membrane binding analysis of the Phox homology domain of phosphoinositide 3-kinase-C2alpha. J. Biol. Chem. **281:**39396–39406.
46. **Suzuki, T., T. Matsusaka, M. Nakayama, T. Asano, T. Watanabe, I. Ichikawa, and M. Nagata.** 2009. Genetic podocyte lineage reveals progressive podocytopenia with parietal cell hyperplasia in a murine model of cellular/collapsing focal segmental glomerulosclerosis. Am. J. Pathol. **174:** 1675–1682.
47. **Turner, S. J., J. Domin, M. D. Waterfield, S. G. Ward, and J. Westwick.** 1998. The CC chemokine monocyte chemotactic peptide-1 activates both the class I p85/p110 phosphatidylinositol 3-kinase and the class II PI3K-C2alpha. J. Biol. Chem. **273:**25987–25995.
48. **van den Berg, J. G., M. A. van den Bergh Weerman, K. J. Assmann, J. J. Weening, and S. Florquin.** 2004. Podocyte foot process effacement is not correlated with the level of proteinuria in human glomerulopathies. Kidney Int. **66:**1901–1906.
49. **Vogel, P., M. S. Donoviel, R. Read, G. M. Hansen, J. Hazlewood, S. J. Anderson, W. Sun, J. Swaffield, and T. Oravecz.** 2009. Incomplete inhibition of sphingosine 1-phosphate lyase modulates immune system function yet prevents early lethality and non-lymphoid lesions. PLoS One **4:**e4112.
50. **Wen, P. J., S. L. Osborne, I. C. Morrow, R. G. Parton, J. Domin, and F. A. Meunier.** 2008. Ca2+-regulated pool of phosphatidylinositol-3-phosphate produced by phosphatidylinositol 3-kinase C2alpha on neurosecretory vesicles. Mol. Biol. Cell **19:**5593–5603.
51. **Wymann, M. P., and R. Marone.** 2005. Phosphoinositide 3-kinase in disease: timing, location, and scaffolding. Curr. Opin. Cell Biol. **17:**141–149.
52. **Xing, J., Z. Zhang, H. Mao, R. G. Schnellmann, and S. Zhuang.** 2008. Src regulates cell cycle protein expression and renal epithelial cell proliferation via PI3K/Akt signaling-dependent and -independent mechanisms. Am. J. Physiol. Renal Physiol. **295:**F145–F152.
53. **Yoshioka, K., N. Sugimoto, N. Takuwa, and Y. Takuwa.** 2007. Essential role for class II phosphoinositide 3-kinase alpha-isoform in Ca2+-induced, Rho- and Rho kinase-dependent regulation of myosin phosphatase and contraction in isolated vascular smooth muscle cells. Mol. Pharmacol. **71:**912–920.
54. **Zhu, J., N. Sun, L. Aoudjit, H. Li, H. Kawachi, S. Lemay, and T. Takano.** 2008. Nephrin mediates actin reorganization via phosphoinositide 3-kinase in podocytes. Kidney Int. **73:**556–566.